

JGR Oceans

RESEARCH ARTICLE

10.1029/2024JC021122

Key Points:

- Increased fractions of Arctic waters decrease aragonite saturation state (Ω_{Ar}) in the upper 200 m, while respiration does so below 200 m
- Decreased Ω_{Ar} of Arctic waters over the last two decades is associated with decreased alkalinity, not additional CO₂
- Significant fractions of Arctic-outflow waters on the west Greenland shelf challenges current knowledge of circulation in Baffin Bay

Supporting Information:

Supporting Information may be found in the online version of this article.

Correspondence to:

T. M. Burgers, tonya.burgers@dfo-mpo.gc.ca

Citation:

Burgers, T. M., Azetsu-Scott, K., Myers, P. G., Else, B. G. T., Miller, L. A., Rysgaard, S., et al. (2024). Unraveling the biogeochemical drivers of aragonite saturation state in Baffin Bay: Insights from the west Greenland continental shelf. *Journal of Geophysical Research: Oceans*, 129, e2024JC021122. https://doi.org/10.1029/2024JC021122

Received 16 MAR 2024 Accepted 6 AUG 2024

Author Contributions:

Conceptualization: Tonya M. Burgers, Tim Papakyriakou
Data curation: Tonya M. Burgers, Kumiko Azetsu-Scott, Brent G. T. Else, Lisa A. Miller, Jean-Éric Tremblay
Formal analysis: Tonya M. Burgers, Kumiko Azetsu-Scott, Wayne Chan
Investigation: Tonya M. Burgers, Paul G. Myers, Søren Rysgaard
Methodology: Tonya M. Burgers, Kumiko Azetsu-Scott, Wayne Chan, Tim Papakyriakou

© 2024. The Author(s).

This is an open access article under the terms of the Creative Commons
Attribution-NonCommercial-NoDerivs
License, which permits use and distribution in any medium, provided the original work is properly cited, the use is non-commercial and no modifications or adaptations are made.

Unraveling the Biogeochemical Drivers of Aragonite Saturation State in Baffin Bay: Insights From the West Greenland Continental Shelf

Tonya M. Burgers^{1,2}, Kumiko Azetsu-Scott³, Paul G. Myers⁴, Brent G. T. Else^{1,5}, Lisa A. Miller^{1,6}, Søren Rysgaard^{1,7,8}, Wayne Chan¹, Jean-Éric Tremblay⁹, and Tim Papakyriakou¹

¹Department of Environment and Geography, Centre for Earth Observation Science, University of Manitoba, Winnipeg, MB, Canada, ²Now at Arctic Aquatic Research Division, Fisheries and Oceans Canada, Winnipeg, MB, Canada, ³Bedford Institute of Oceanography, Fisheries and Oceans Canada, Dartmouth, NS, Canada, ⁴Department of Earth and Atmospheric Sciences, University of Alberta, Edmonton, AB, Canada, ⁵Department of Geography, University of Calgary, Calgary, AB, Canada, ⁶Institute of Ocean Sciences, Fisheries and Oceans Canada, Sidney, BC, Canada, ⁷Department of Biology, Arctic Research Centre, Aarhus University, Aarhus, Denmark, ⁸Greenland Climate Research Centre, Greenland Institute of Natural Resources, Nuuk, Greenland, ⁹Québec-Océan and Takuvik Joint International Laboratory, Départment de Biologie, Université Laval, Québec, QC, Canada

Abstract This study investigates the biogeochemical drivers of aragonite saturation state (Ω_{Ar}) in Baffin Bay, with a focus on the relatively undersampled west Greenland shelf. Our findings reveal two main depthdependant processes controlling the spatial distribution of Ω_{Ar} in Baffin Bay; within the upper 200 m, lower Ω_{Ar} coincides with increasing fractions of Arctic-outflow waters, while below 200 m organic matter respiration decreases Ω_{Ar} . A temporal analysis comparing historical measurements from 1997 and 2004 with our 2019 data set reveals a significant decrease in the Ω_{Ar} of Arctic-outflow waters, coinciding with reduced total alkalinity (TA). However, no discernible anthropogenic ocean acidification signal is identified. Significant Arctic water fractions (20%–40%) are found to be present on the west Greenland shelf, associated with reduced TA and Ω_{Ar} . A numerical modeling simulation incorporating a passive tracer demonstrates that periodic changes in wind direction lead to a switch from onshore to offshore Ekman transport along the Baffin Island current, transporting Arctic waters toward the west Greenland shelf. This challenges the conventional understanding of Baffin Bay's circulation and underscores the need for further research on the region's physical oceanography. Based on salinity-TA relationships, surface waters on the west Greenland shelf have a significantly lower meteoric TA end-member compared to waters of the Baffin Island Current in western Baffin Bay. The low eastern TA freshwater end-member agrees well with recent glacial meltwater TA measurements, suggesting that glacial meltwater is the main freshwater source to surface waters on the west Greenland shelf.

Plain Language Summary Baffin Bay, with its complex interplay of Atlantic and Arctic water masses, is particularly susceptible to ongoing ocean acidification, mainly due to the presence of relatively fresh and low-alkalinity Arctic waters. To date measurements of the inorganic carbon system in Baffin Bay have primarily been captured at key entrance and exit gateways, and on the Canadian side of the bay, leaving the west Greenland shelf relatively undersampled. This study provides a bay-wide perspective of the main factors influencing aragonite saturation state (Ω_{Ar} ; an indicator of ocean acidification impacts on marine calcifying organisms) across Baffin Bay, including the west Greenland shelf. We found that within the upper 200 m, low Ω_{Ar} coincides with increased presence of Arctic waters, while below 200 m the breakdown of organic matter decreases Ω_{Ar} . Historical data from 1997 and 2004 compared to our 2019 measurements show a significant drop in Ω_{Ar} of Arctic waters, but no clear signal of anthropogenic ocean acidification was observed. Surprisingly, the west Greenland shelf has significant fractions (20%–40%) of Arctic water. A numerical modeling simulation suggests that periodic changes in wind direction can transport Arctic waters from across Baffin Bay, challenging our traditional understanding of the bay's circulation.

1. Introduction

With ongoing increases in atmospheric carbon dioxide (CO_2) concentrations, the surface ocean continues to absorb more CO_2 through air-sea gas exchange as it attempts to achieve equilibrium with the atmosphere. Current

BURGERS ET AL. 1 of 21





Journal of Geophysical Research: Oceans

10.1029/2024JC021122

Resources: Brent G. T. Else, Lisa A. Miller, Jean-Éric Tremblay, Tim Papakyriakou Supervision: Tim Papakyriakou Visualization: Paul G. Myers Writing – original draft: Tonya M. Burgers Writing – review & editing: Kumiko Azetsu-Scott, Paul G. Myers, Brent G. T. Else, Lisa A. Miller, Søren Rysgaard, Wayne Chan, Jean-Éric Tremblay, Tim Papakyriakou estimates suggest that the global surface ocean has taken up roughly one quarter of all anthropogenic CO_2 emissions over the past decade (Friedlingstein et al., 2023). Although this process is beneficial in reducing the magnitude of the greenhouse effect in the atmosphere, it also results in major changes to ocean chemistry. Specifically, increases in dissolved CO_2 concentrations cause decreases in seawater pH (leading to the process name "ocean acidification"), and simultaneous increases in the solubility of calcium carbonate (CaCO₃) minerals, which many marine calcifying species utilize to form their shells and skeletons (AMAP, 2013; Doney et al., 2009).

The saturation state (Ω) of CaCO₃ minerals is a measure of the mineral's tendency to dissolve under certain chemical conditions, and is defined as:

$$\Omega = \left[\text{Ca}^{2+} \right] \left[\text{CO}_3^{2-} \right] / K_{sp}^*$$

where $[\mathrm{Ca^{2+}}]$ and $[\mathrm{CO_3^{2-}}]$ are the dissolved concentrations of calcium and carbonate ions in seawater, respectively, and K_{sp}^* is the conditional solubility product of $\mathrm{CaCO_3}$ in seawater (dependent on seawater temperature, salinity, and pressure). The two most common polymorphs of $\mathrm{CaCO_3}$ that are produced by marine calcifying organisms are calcite and aragonite, with their saturation states denoted as Ω_{Ca} and Ω_{Ar} , respectively. Aragonite is more soluble (i.e., has a higher solubility product) than calcite (Mucci, 1983), meaning that aragonite will dissolve under higher pH conditions relative to calcite. If $\Omega > 1$ then the seawater is considered "supersaturated," and the $\mathrm{CaCO_3}$ mineral is stable, but if $\Omega < 1$ the seawater is "undersaturated" and $\mathrm{CaCO_3}$ minerals will tend to dissolve.

The Arctic Ocean has been found to be especially vulnerable to ocean acidification, because of high freshwater inputs, cold seawater temperatures, and declining sea-ice cover (AMAP, 2018). Freshwater inputs from river runoff, sea-ice melt, and glacial meltwater are all characterized by low total alkalinity (TA) compared to seawater and therefore reduce the seawater's buffering capacity against ocean acidification, leading to greater decreases in pH and Ω for every unit of added CO_2 . Even Pacific-origin seawater, which enters the Arctic Ocean via the Bering Strait, has a lower salinity than Atlantic-origin seawater and therefore also has relatively low TA. Pacific waters also contain more dissolved inorganic carbon (DIC) due to the accumulation of respiration products along the global thermohaline circulation route. Hence, Pacific waters are predisposed toward low pH and Ω values due to their relatively low TA:DIC ratio (Azetsu-Scott et al., 2010; Shadwick et al., 2011; Yamamoto-Kawai et al., 2013).

Baffin Bay (Sannirutiup Imanga in Inuktitut) is a seasonally ice-covered sea in the eastern Canadian Arctic, with a complex interplay of Atlantic and Arctic-outflow waters. Much like the greater Arctic Ocean, Baffin Bay is particularly susceptible to ocean acidification (AMAP, 2018; Azetsu-Scott et al., 2010). Arctic waters that enter Baffin Bay from the north are predominantly Pacific-source waters, which are already prone to low pH and Ω . On top of this, additional freshwater inputs may be added within Baffin Bay from melting sea ice or glacial meltwater, further decreasing TA. In fact, Bamber et al. (2018) found that Baffin Bay currently receives the largest freshwater flux anomalies (compared to the 1,960–1,990 mean) from land ice compared to other seas surrounding Greenland, and continues to show the steepest rates of acceleration in these fluxes. Baffin Bay is also a very biologically productive marine environment (Burgers et al., 2020; Klein et al., 2002; Krawczyk et al., 2021), contributing to organic matter export and deep respiration by heterotrophic organisms, releasing dissolved inorganic carbon (DIC) while decreasing TA, leading to decreases in Ω of the deep and bottom waters.

In light of these vulnerabilities to ocean acidification, Azetsu-Scott et al. (2010) provided the first baseline measurements of Ω_{Ca} and Ω_{Ar} throughout the outflow shelves of the eastern Canadian Arctic (including Baffin Bay) between 2003 and 2005. Their measurements showed a west-to-east deepening of the aragonite saturation horizon ($\Omega_{Ar}=1$) across Baffin Bay, from approximately 200 m depth in the west to 500 m in the east. This gradient was found to be due to the presence of Arctic-outflow waters in the upper water column of western Baffin Bay, with its greater Pacific water influence contributing to lower Ω_{Ar} values (Azetsu-Scott et al., 2010; Yamamoto-Kawai et al., 2013).

With rising air temperatures (Rantanen et al., 2022), declining sea-ice thickness (Landy et al., 2017), a longer openwater season (Ballinger et al., 2022), and increasing freshwater inputs both from glacial discharge (Bamber et al., 2018; Mouginot et al., 2019) and increasingly fresh surface waters exported from the Arctic Ocean (Carmack et al., 2016; Haine et al., 2015), conditions in Baffin Bay are changing rapidly. Such drastic changes will have

BURGERS ET AL. 2 of 21

from https://agupubs.onlinelibrary.wiley.com/doi/10.1029/2024JC021122 by Kathleen Mary Stafford - Oregon State University, Wiley Online Library on [2907/2025]. See the Terms

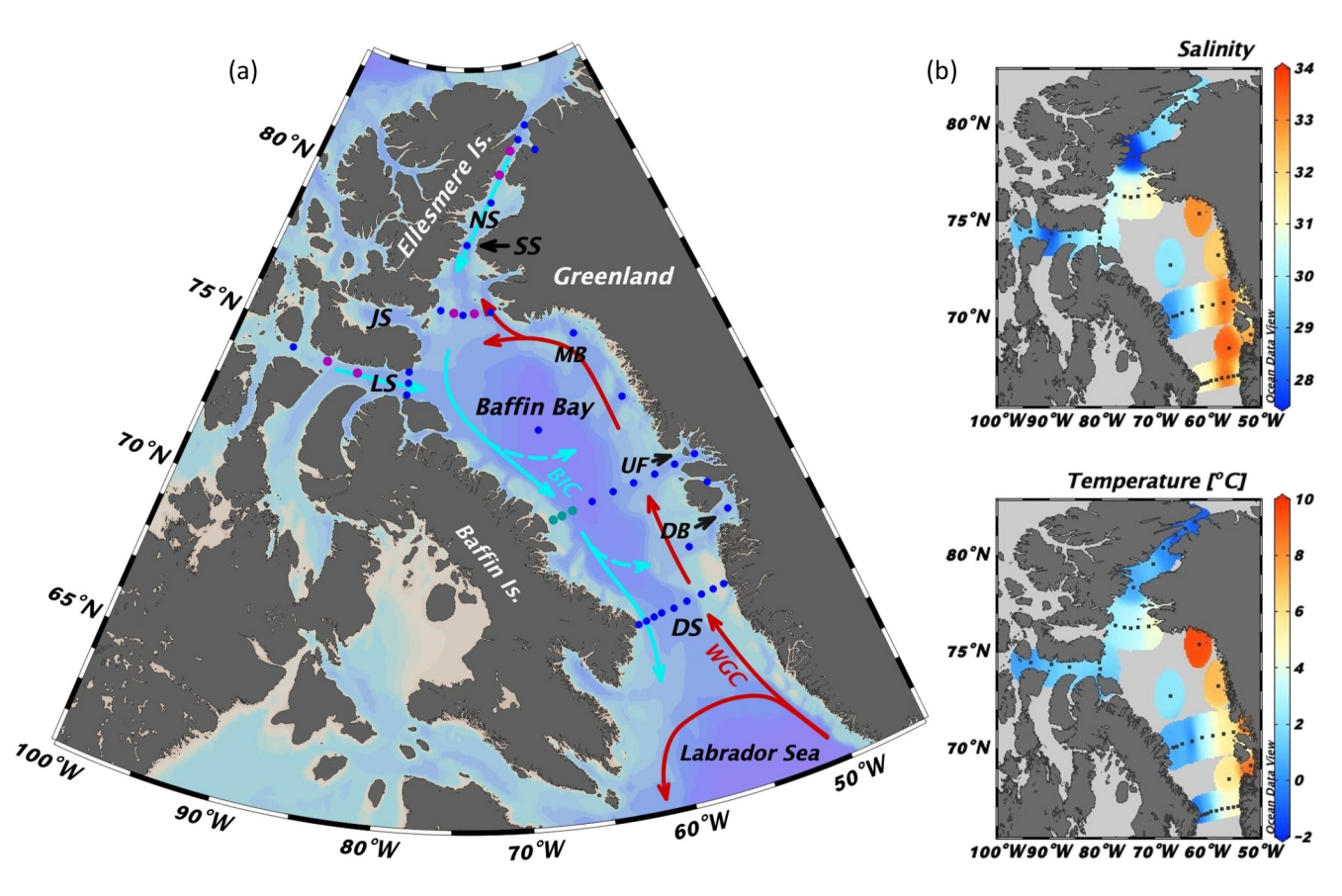


Figure 1. (a) Map of the study area, with water column sampling stations indicated as colored dots. At stations plotted as blue dots samples were collected for inorganic carbon throughout the water column at standard sampling depths. At purple station locations inorganic carbon samples were only collected at the surface and 10 m depths. Alkalinity samples from the green stations were excluded from our discussion, because of an analytical malfunction (see Section 3.1). Abbreviations: Baffin Island Current (BIC), West Greenland Current (WGC), Nares Strait (NS), Smith Sound (SS), Jones Sound (JS), Lancaster Sound (LS), Davis Strait (DS), Uummannaq Fjord (UF), Disko Bay (DB), and Melville Bay (MB). (b) Surface distributions of salinity (on the practical scale, top) and temperature in Baffin Bay.

consequences for the marine ecosystem in the bay, and for biogeochemical processes such as air-sea CO_2 exchange, primary production, and ongoing ocean acidification. It is therefore important to keep monitoring the biogeochemistry of the region, especially in light of its important ecological areas (such as the North Water polynya) and economic interests (e.g., the west Greenland shrimp fishery; AMAP, 2018). In past oceanographic studies of Baffin Bay, there have been few measurements over the west Greenland shelf (the eastern portion of Baffin Bay). Often the only location to have been sampled fully from west to east is Davis Strait in southern Baffin Bay. The coastline of west Greenland northwards of Davis Strait houses many large and fast-flowing tidewater glaciers, and this region has been shown to display greater glacial ice discharge rates than other coastal regions of Greenland (Mouginot et al., 2019). It is therefore very important to investigate whether such large glacial ice and/or freshwater fluxes may be impacting the marine carbonate chemistry of the west Greenland shelf.

In this investigation we present recent (July and August 2019) measurements of the marine carbonate system, along with stable oxygen isotope ratios (δ^{18} O) and nutrient concentrations across Baffin Bay, including many sampling locations along the west Greenland shelf between 67°N and 76°N (Figure 1). The objectives of this study have been to: (a) investigate the importance of biogeochemical processes on the west Greenland shelf in controlling the distribution of $\Omega_{\rm Ar}$ within Baffin Bay; and (b) compare our 2019 measurements with those presented in Azetsu-Scott et al. (2010) from 1997 and 2004 to identify any temporal trends in $\Omega_{\rm Ar}$.

2. Oceanographic Setting

The distribution of water masses in Baffin Bay is governed by an overall cyclonic circulation, which consists of two major currents (Figure 1a): the Baffin Island Current (BIC) and the West Greenland Current (WGC). The BIC

BURGERS ET AL. 3 of 21

com/doi/10.1029/2024JC021122 by Kathleen

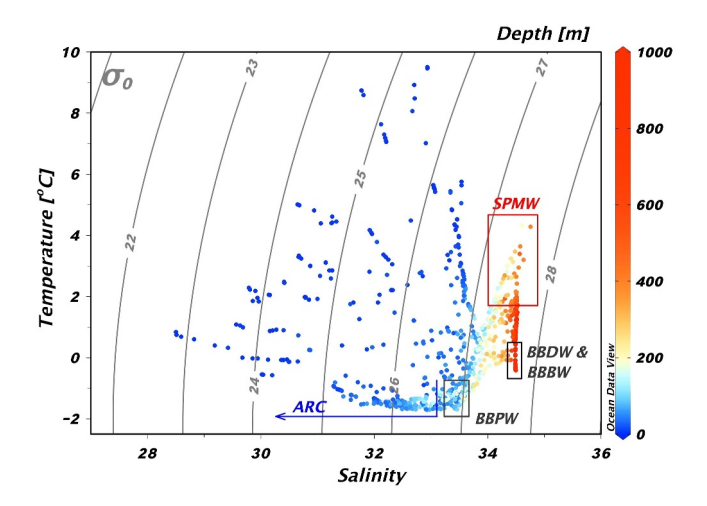


Figure 2. Temperature-salinity (TS) plot for the Baffin Bay region during July and August 2019. Thin gray lines represent isopycnals. For station locations see Figure 1. Major water masses are identified by rectangles on the TS-diagram. Abbreviations: Arctic water (ARC), Baffin Bay Polar Water (BBPW), Subpolar Mode Water (SPMW), Baffin Bay Deep Water (BBDW), Baffin Bay Bottom Water (BBBW).

transports relatively cold and fresh Arctic outflow waters from the channels of the Canadian Arctic Archipelago (CAA) southwards along the Baffin Island continental slope, and into the Labrador Sea. The northward flowing WGC advects relatively warm and saline waters from the North Atlantic into eastern Baffin Bay along the west Greenland continental shelf and slope (Curry et al., 2014; Tang et al., 2004; see Figure 1b). These two current systems create different water mass assemblies in eastern and western Baffin Bay, and also affect the timing of sea ice formation and retreat across Baffin Bay. Due to the relatively warm surface water temperatures of the WGC, sea ice retreats much earlier (April) in eastern Baffin Bay than to the west (July). All of Baffin Bay is generally ice free from July to October (Bi et al., 2019). When the data for this study were collected (July and August 2019), all of Baffin Bay was essentially ice free (Figure S1 in Supporting Information S1).

In the water column of eastern Baffin Bay, we identify two main water masses (Figure 2): (a) Baffin Bay Polar Water (BBPW) with $T < -1^{\circ}C$ and 33.4 < S < 33.65, located between depths of $40{\text -}100$ m, and (b) Subpolar Mode Water (SPMW) displaying $T > 0^{\circ}C$, S > 34.3, and located at depths between 200 and 500 m (Rysgaard et al., 2020). BBPW is a winter mode water (i.e., formed by winter convection) that is characterized by temperatures near the freezing point, and has been commonly observed along the west Greenland shelf north of Disko Bay (Bâcle et al., 2002; Burgers et al., 2017;

Rysgaard et al., 2020; Tang et al., 2004). Sporadically, BBPW has also been observed as far south as 64°N along the west Greenland shelf (Mortensen et al., 2022). SPMW is formed as a winter mode water in the subpolar North Atlantic before flowing around southern Greenland in the Irminger Current, and continuing northwards into Baffin Bay with the WGC (Rysgaard et al., 2020). In previous literature SPMW has been referred to as Atlantic water, Irminger water, or West Greenland Irminger water (Azetsu-Scott et al., 2012; Lin et al., 2018; Myers et al., 2009). As SPMW transits cyclonically around Baffin Bay it becomes slightly cooler and fresher as it mixes with Arctic outflow waters from the CAA.

In western Baffin Bay, BBPW and SPMW are still present but are located at greater depths in the water column and are overlain by Arctic Ocean outflow waters (ARC, Figure 2). Along the Baffin Island continental slope BBPW is generally found near 150 m depth, and SPMW between depths of 300 and 700 m. Arctic outflow waters are present throughout the upper 150 m in western Baffin Bay, displaying $T < 0^{\circ}C$ and S < 33.3. These Arctic waters represent a mixture composed of primarily Pacific-origin halocline waters (31 > S > 33.1), with contributions from sea-ice meltwater and meteoric waters from pan-Arctic rivers, glacial melt, and net precipitation (Carmack et al., 2016). Arctic waters entering Baffin Bay are primarily of Pacific-origin, as deeper Atlantic-origin water masses are held back by the shallow sills within the channels of the CAA. Only Nares Strait has a sill deep enough (approximately 220 m in Kane Basin; Melling et al., 2008) to allow the continuation of some modified-Atlantic waters from the Arctic Ocean to flow southwards into northern Baffin Bay (Azetsu-Scott et al., 2010).

The deep basin in central Baffin Bay reaches depths of approximately 2,400 m, and here the water at depth is composed of Baffin Bay Deep water (BBDW) and Baffin Bay Bottom water (BBBW). Salinity is quite stable throughout these water masses, at 34.5. BBDW has a temperature of 0° C and is found at depths between 1,200 and 1,800 m (Curry et al., 2011), whereas BBBW has a temperature of -0.4° C, and is found at depths greater than 1,800 m. A recent study by Zeidan et al. (2022) estimated the residence time of BBDW to be between 360 and 690 years based on radiocarbon (Δ^{14} C) values, indicating that carbon is likely stored for centuries in deep Baffin Bay.

3. Methods

3.1. Sampling and Sample Analysis

Sampling for this study was conducted between 5 July and 15 August during Leg 2 of the 2019 ArcticNet scientific cruise aboard the CCGS *Amundsen*. At each sampling station seawater was collected with 12L Niskin-type bottles mounted on a rosette system equipped with a SeaBird 911plus CTD, and a dissolved oxygen sensor (SeaBird SBE-43). Discrete water samples were collected for the determination of salinity, stable oxygen isotope

BURGERS ET AL. 4 of 21

ratios (δ^{18} O), nutrients (including nitrate + nitrite, ammonium, phosphate and silicate), dissolved inorganic carbon (DIC), and total alkalinity (TA). Discrete samples were collected at standard depths of: 2, 5, 10, 20, 30, 50, 70, 100, 150, 200, 250, 300, 400, 600, 800, 1,000, and 1,200 m. Only two stations in central Baffin Bay had bottom depths deeper than 1,200 m, and were sampled at 100 m intervals between depths of 1,400 and 2,300 m. At a subset of stations DIC and TA samples were only collected at the surface and 10 m depth, these stations are indicated in Figure 1a by purple dots. Bottle salinity measurements were made onboard using a Guideline Autosal model 8,400 salinometer provided by Amundsen Science, and reported using the practical salinity scale (PSU).

Nutrient samples were collected directly from the rosette bottles with syringes, filtered through a Swinnex-mounted Whatman GF/F, and captured in acid-cleaned polyethylene tubes. Concentrations of nitrate + nitrite, ammonium, phosphate, and silicate were measured colorimetrically using a Bran and Luebbe AutoAnalyzer III within a few hours of collection. Working standards were prepared at each station and checked against certified reference material (KANSO CRM) inserted in the sample runs. Analytical detection limits were $0.03~\mu\text{M}$ for nitrate (obtained by the difference between nitrite and nitrate + nitrite), $0.02~\mu\text{M}$ for nitrite, $0.05~\mu\text{M}$ for phosphate, and $0.1~\mu\text{M}$ for silicate. Ammonium concentrations were determined using the method of Holmes et al. (1999) with a detection limit of $0.02~\mu\text{M}$. The precision of triplicate nutrient measurements under the range of concentrations observed was the same as, or better than, the detection limit for each nutrient.

Samples for δ^{18} O were analyzed at the University of Calgary using an integrated off-axis cavity absorption spectrometer (Los Gatos Research, LGR, Triple Liquid Water Isotope Analyzer, model 912-0032). The LGR analyzer was standardized every 4 samples with in-house standards that were calibrated against VSMOW2 (Vienna Standard Mean Ocean Water 2) and SLAP2 (Standard Light Antarctic Precipitation 2) standards. For each sample, 8 replicates were sequentially measured through an auto-injector. The first 4 measurements were discarded to eliminate memory effects, and the average of the last 4 measurements was used for isotope ratio calculations. The analytical precision (2σ) of the δ^{18} O measurements was better than \pm 0.2‰.

Samples for DIC and TA determination were collected and analyzed following standard protocols (Dickson et al., 2007), with duplicates collected from at least one bottle on each rosette cast. Samples were collected in 250or 500-mL borosilicate glass bottles, preserved with 100 μL of a saturated HgCl₂ solution, capped with ground glass stoppers greased with Apiezon M, and sealed with clips and elastic closures or with electrical tape. Samples were stored in the dark at 4°C until analysis at either the Bedford Institute of Oceanography (BIO) in Dartmouth, Nova Scotia or the Institute for Ocean Sciences (IOS) in Sidney, British Columbia. Both labs analyzed samples for DIC coulometrically, followed by TA determination from the same bottle using potentiometric titrations. At BIO samples were analyzed for DIC using a modified SOMMA (Johnson et al., 1993), whereas IOS measured DIC using a VINDTA 3D (MARIANDA). At both labs TA was analyzed using custom-built open-cell titration systems (see Punshon et al., 2019, for further specifics of sample analysis at BIO). Measurements from both labs were calibrated against certified reference materials provided by Andrew Dickson (Scripps Institute of Oceanography). Analysis of duplicate DIC and TA samples at IOS indicated precisions of ±1 μmol kg⁻¹ and $\pm 2 \,\mu$ mol kg⁻¹, respectively. Similarly, the DIC and TA samples analyzed at BIO had precisions of $\pm 1 \,\mu$ mol kg⁻¹ and ±3 µmol kg⁻¹, respectively. A subset of the TA measurements were affected by a clogged tube in the titration system, causing insufficient sample to be dispensed into the titration cup. These TA values have been flagged as bad, and excluded from further data analysis. The station locations without TA values due to this issue are shown in green in Figure 1a.

We computed the aragonite saturation state (Ω_{Ar}) from the DIC and TA measurements using the R package Seacarb (Gattuso et al., 2021) and employing the equilibrium constants $(K_1$ and $K_2)$ of Sulpis et al. (2020), which are valid for seawater temperatures down to -1.7° C, and are therefore better suited to cold high-latitude regions. Uncertainties in calculated Ω_{Ar} values due to measurement uncertainties in DIC, TA, and phosphate and silicate concentrations were assessed using the error propagation routine of Orr et al. (2018). To assess the variability in Ω_{Ar} due to the choice of equilibrium constants, we also calculated Ω_{Ar} using the constants of Lueker et al. (2000), which are generally recommended by best practices for oceanic carbonate system measurements (Dickson et al., 2007), but were found by Sulpis et al. (2020) to underestimate pK_1 and pK_2 in seawater temperatures below 8°C. It is important to note that differences in Ω_{Ar} values due to the choice of equilibrium constants are larger than the errors caused by the propagation of measurement precisions (Table 1), and based on the results of an unpaired t-test the difference is statistically significant (p < 0.01).

BURGERS ET AL. 5 of 21

Average Uncertainties in Calculated Ω_{Ar} Due To Measurement Error in Temperature, Salinity, Phosphate (P), Silicate (Si), Dissolved Inorganic Carbon (DIC) and Total Alkalinity (TA)

	Temp (° C) (×10 ⁻⁵)	Salinity (×10 ⁻⁵)	P (×10 ⁻⁵)	Si (×10 ⁻⁶)	DIC	TA	Cumulative measurement precision error	Difference in equilibrium constants (L00–S20)
$\Delta\Omega_{ m Ar}$	7.9 ± 1.6	8.8 ± 5.1	40 ± 7.5	13 ± 6.5	0.0073 ± 0.0013	0.018 ± 0.0049	0.019 ± 0.0039	0.025 ± 0.0079

Note. Also listed is the cumulative uncertainty due to measurement errors in the formerly listed parameters, and the average difference in calculated Ω_{Ar} due to the choice of equilibrium constants between Lueker et al. (2000) and Sulpis et al. (2020), denoted as L00 and S20, respectively. All uncertainty estimates in Ω_{Ar} were calculated using the error propagation routine of Orr et al. (2018).

3.2. Historical Data Sets

Historical data sets of the marine carbonate system in Baffin Bay were downloaded from GLODAPv2.2022 (Lauvset et al., 2022). Measurements of DIC and TA from cruises in 1997, 2003 and 2004 were accessed (expocodes 18SN19970803, 32H120030721, and 316N20040922, respectively). The data set from 1997 was collected in August from the CCGS *Louis S. St. Laurent*, the 2003 data set was collected in July and August from the R/V Healy, and the 2004 data set was collected in September from R/V *Knorr*. Herein, we re-calculated $\Omega_{\rm Ar}$ values from these historical data sets using the equilibrium constants of Sulpis et al. (2020) in order to compare them with $\Omega_{\rm Ar}$ values from the 2019 cruise.

3.3. Freshwater Partitioning

We distinguish fractions of sea-ice meltwater (F_{SIM}), meteoric water (F_{MW}), Arctic water (F_{ARC}) and Atlantic water (F_{ATL}) using measurements of salinity, δ^{18} O, dissolved inorganic nitrogen (DIN = $NO_3^- + NO_2^- + NH_4^+$), and phosphate (P). Our methodology closely follows that of Azetsu-Scott et al. (2012), but employs DIN:P regression relationships unique to our data set. In Baffin Bay there are two separate types of seawater that interact: Arctic and Atlantic waters, which enter the bay from the north through channels of the CAA, and from the south through Davis Strait, respectively. Arctic waters are mainly composed of modified Pacific waters, that were impacted by denitrification in the oxygen minimum zones of the North Pacific and in the benthos of the shallow Bering and Chukchi shelves (Cooper et al., 1997; Jones et al., 1998; Yamamoto-Kawai et al., 2008). Therefore, Arctic waters display a relatively low DIN:P ratio compared to Atlantic waters. In this study, we first determine the ratio of Arctic and Atlantic seawater in a particular sample using the unique DIN:P relationships for each seawater type. The resulting ratio is then used to calculate a seawater end-member value for each sample, using known Arctic and Atlantic water end-member properties (Table 2). Finally, fractions of sea-ice meltwater, meteoric water, and seawater are determined for each sample using salinity and δ^{18} O measurements in a three end-member mixing model.

Figure 3 shows the DIN:P relationships defined for Arctic and Atlantic waters in Baffin Bay using this data set from summer 2019. The Atlantic water line was determined from samples with S > 33.3, $T > 0^{\circ}$ C, and depths less than 1,000 m to eliminate BBDW and BBBW where benthic denitrification is known to occur (Lehmann et al., 2019). It is worth noting that our definition of Atlantic water within Baffin Bay represents a modified (relatively fresh) version of pure Atlantic water, with modified nutrient ratios. Therefore, our calculated water mass fractions will differ from other studies which have applied the nutrient relationship of Jones et al. (1998), defined using observations from the St. Anna Trough. The Arctic water line was determined from samples with $S \le 33.3$ and $T < 0^{\circ}$ C, representing mainly Pacific halocline waters and any additional freshwater inputs (e.g., sea-ice melt, river runoff, and glacial melt) that are exiting the Arctic Ocean. The ratio of Arctic and Atlantic

 Table 2

 End-Member Values and Their Uncertainties Used in Freshwater Decomposition

	Atlantic water ^a	Arctic water ^b	Sea-ice meltwater ^a	Meteoric water ^{a,c}
Salinity	34.8 ± 0.1	32 ± 1	4 ± 1	0
δ^{18} O (‰)	0.19 ± 0.06	-2.0 ± 0.5	0.63 ± 0.14	-20 ± 2

^aAzetsu-Scott et al. (2012). ^bCalculated from the observations in this study (averages of samples with S ≤ 33.3 and T < 0°C). ^cFairbanks (1982).

BURGERS ET AL. 6 of 21

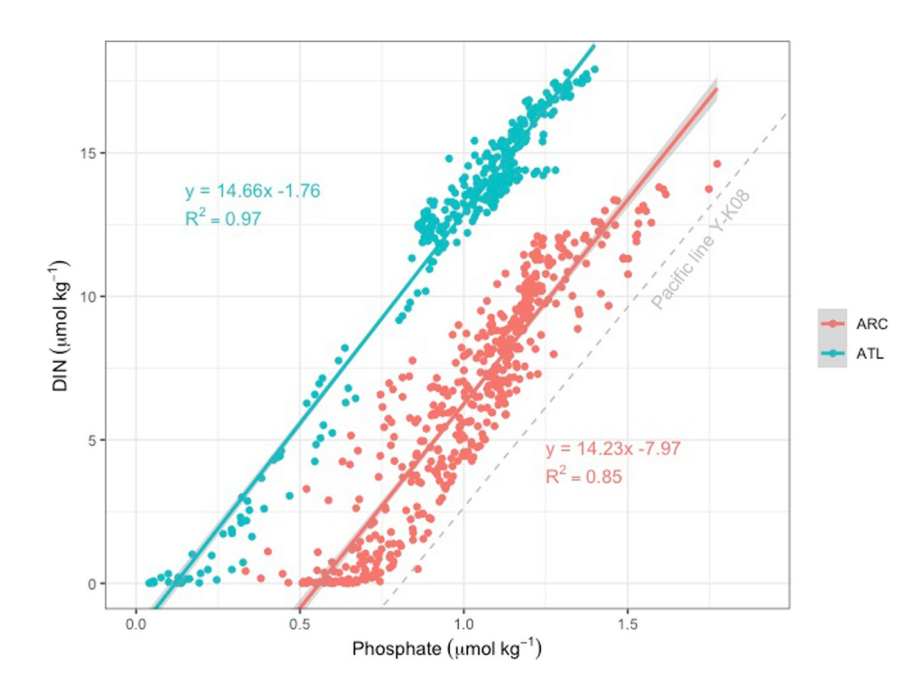


Figure 3. Linear regression relationships of dissolved inorganic nitrogen (DIN) versus phosphate for Atlantic waters and Arctic waters in Baffin Bay. The Atlantic water line (blue line) was determined from samples with S > 33.3 and $T > 0^{\circ}$ C and depths <1,000 m (blue dots). The Arctic water line (red line) was determined from samples with $S \le 33.3$ and $T < 0^{\circ}$ C (red dots). The 95% confidence intervals for each regression line are shown as shaded gray bands. The Pacific line from the previous study of Yamamoto-Kawai et al. (2008) is also shown for comparison.

seawater in a particular sample is determined by the relative distance of the measured DIN:P ratio between the two regression lines:

$$P_{ARC} = (DIN_{obs} + 7.97)/14.23$$
 (1)

$$P_{\text{ATL}} = (\text{DIN}_{\text{obs}} + 1.76)/14.66$$
 (2)

$$f_{ARC} = (P_{ATL} - P_{obs})/(P_{ATL} - P_{ARC})$$
(3)

$$f_{\text{ATL}} = 1 - f_{\text{ARC}} \tag{4}$$

where $P_{\rm ARC}$ and $P_{\rm ATL}$ represent the phosphate concentrations expected, based on the observed concentration of DIN, if the sample falls along the Arctic or Atlantic water line, respectively (Equations 1 and 2). If the observed phosphate concentration ($P_{\rm obs}$) matches that predicted by the Arctic water line ($P_{\rm ARC}$), it will yield an Arctic water fraction of 1 ($f_{\rm ARC}=1$). If $P_{\rm obs}$ falls somewhere between the Arctic and Atlantic water lines, it will yield a lower $f_{\rm ARC}$ and higher $f_{\rm ATL}$ (Equations 3 and 4). If $P_{\rm obs}$ falls to the left of the Atlantic line in Figure 2, creating a negative $f_{\rm ARC}$ value, we assume there is no Arctic water and $f_{\rm ATL}=1$. Similarly, if $P_{\rm obs}$ falls to the right of the Arctic line, we assume there is no Atlantic water and $f_{\rm ARC}=1$.

In this method, the slopes of the two source water lines must be equal, otherwise there is no unique solution for the ratio of the two seawater types (Azetsu-Scott et al., 2012). This fact is often overlooked in other studies using a Pacific water line based on DIN:P relationships, whose slopes are not the same as that of the Atlantic water line. The slopes of the two regression lines in this study were tested using an ANOVA and were found to be equal within statistical uncertainty. Uncertainties in the determined seawater composition of each sample arise from the errors associated with the determination of the Arctic and Atlantic lines. The 95% confidence intervals for each line are shown in Figure 3 (as shaded gray bands), and indicate that both lines are robust. Overall, uncertainties due to the regression estimates are very low, with mean uncertainties in $f_{\rm ARC}$ and $f_{\rm ATL}$ being less than 0.01. A maximum uncertainty of 0.04 was associated with the Arctic line at high nutrient concentrations ($P > 1.3 \ \mu \rm mol \ kg^{-1}$). Another key assumption made when using this approach is that the biological production

BURGERS ET AL. 7 of 21

Once preliminary fractions of Atlantic and Arctic waters are known, they are used to define the salinity and $\delta^{18}O$ of the seawater end-member (SW) in a three end-member mixing model (Equations 5–7). Once fractions of SIM, MW and SW have been estimated, the Pacific and Atlantic water fractions are recalculated (final F_{ARC} and F_{ATL} values in Equations 8 and 9). End-member values of salinity (S) and $\delta^{18}O$ and their uncertainties are summarized in Table 2.

$$F_{SIM}S_{SIM} + F_{MW}S_{MW} + F_{SW}\left[f_{ARC}S_{ARC} + f_{ATL}S_{ATL}\right] = S_{obs}$$

$$(5)$$

$$F_{SIM}\delta^{18}O_{SIM} + F_{MW}\delta^{18}O_{MW} + F_{SW}\left[f_{ARC}\delta^{18}O_{ARC} + f_{ATL}\delta^{18}O_{ATL}\right] = \delta^{18}O_{obs}$$
 (6)

$$F_{SIM} + F_{MW} + F_{SW} = 1 (7)$$

$$F_{ARC} = f_{ARC} F_{SW}$$
 (8)

$$F_{ATL} = f_{ATL} F_{SW} \tag{9}$$

Sensitivity of the calculated water-type fractions to the uncertainty in end-member values (Table 2) was examined using a Monte Carlo simulation. Each of the end-member values in Table 2 (excluding S_{MW} , which is 0 ± 0) was represented by one thousand random numbers, normally-distributed according to their stated mean and standard deviation. By solving the three end-member mixing model (Equations 5–9) for each of the randomly created end-member values, a distribution of one thousand possible water-type fractions for F_{ARC} , F_{ATL} , F_{SIM} , and F_{MW} was created. The standard deviations of these distributions are plotted in Figures S2 and S3 of Supporting Information S1, representing the absolute uncertainties in calculated water-type fractions. It is important to note that the absolute uncertainties are directly related to the water-type fractions, and therefore can be less important than the relative uncertainties (shown in Figures S4 and S5 of Supporting Information S1), represented by the coefficient of variation (CV = standard deviation/mean). For example, the largest absolute uncertainties in F_{ARC} are observed in the surface waters of western Baffin Bay, Lancaster Sound and northern Nares Strait, simply because those are the areas where F_{ARC} is highest (>0.85, see Figure 4c). On the other hand, the CV of F_{ARC} is still quite low (<0.05) in those areas, and therefore those F_{ARC} values are actually robust. In contrast, high CV (>0.9) are associated with most positive F_{SIM} values, indicating that F_{SIM} estimates throughout the study region are less reliable.

3.4. Passive Tracer Analysis With NEMO

A passive tracer analysis of Pacific-source water transport was conducted using a coupled ocean and sea-ice model based on the Nucleus for European Modeling of the Ocean (available at https://www.nemo-ocean.eu) Version 3.4 (Madec, 2008). The sea-ice module used here is the Louvain-la-Neuve sea ice Model Version 2 with an elastic-viscous-plastic rheology (Hunke & Dukowicz, 1997), including both thermodynamic and dynamic components (Bouillon et al., 2009; Fichefet & Morales Maqueda, 1997). The entire model domain covers the Arctic Ocean and the Northern Hemisphere Atlantic (ANHA) with two open boundaries, one close to Bering Strait in the Pacific Ocean and the other one at 20°S across the Atlantic Ocean, at 1/12° resolution. Benefiting from the tripolar grid, ANHA12 has a horizontal grid spacing of less than 4.5 km in most regions in the Arctic Ocean. In the vertical, there are 50 geopotential levels with higher resolution focused on the upper ocean. Level thickness smoothly transitions from approximately 1 m at the surface (22 levels for the top 100 m) to 458 m at the last level. Partial steps (Barnier et al., 2006) are enabled to better resolve the seafloor. Further detail on this configuration and experiment, including model evaluation, are given by Hu et al. (2019) and Courtois et al. (2020).

The simulations are integrated from 1 January 2002–31 December 2019. This time period was chosen to allow enough spin-up time for the Pacific water tracer to reach and build up in Baffin Bay, and the results near the end of the simulation can be compared to our observations in 2019. At the surface, the model is driven with high temporal (hourly) and spatial resolution (33 km) atmospheric forcing data from the Canadian Meteorological Center Global Deterministic Prediction System ReForecasts data set (Smith et al., 2004). To trace Pacific water

BURGERS ET AL. 8 of 21

onlinelibrary.wiley.com/doi/10.1029/2024JC021122 by Kathleen Mary Stafford - Oregon State University

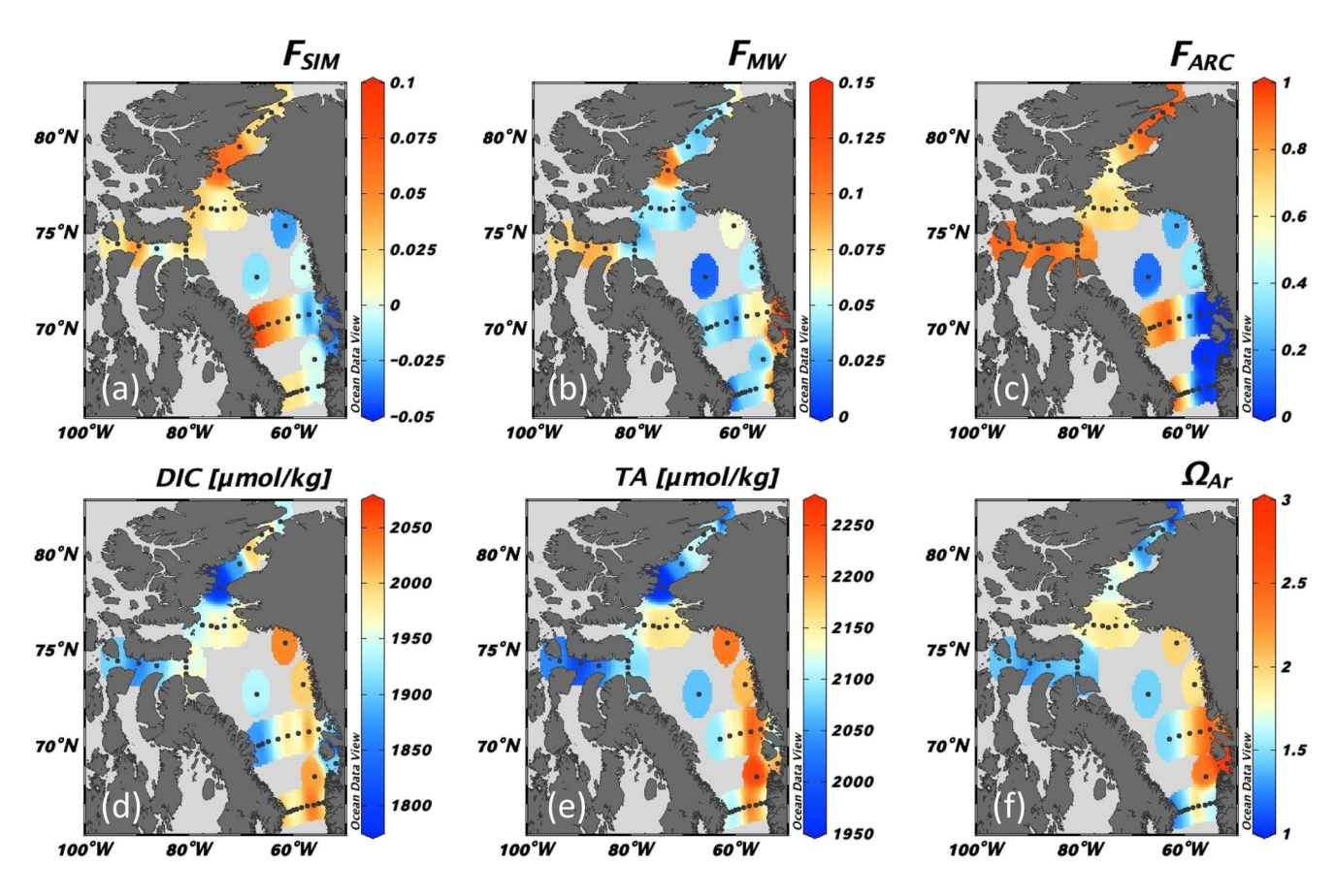


Figure 4. Surface distributions of water-type fractions, (a) fraction of sea-ice meltwater, (b) fraction of meteoric water, (c) fraction of Arctic water, and inorganic carbon system parameters, (d) dissolved inorganic carbon concentration, (e) total alkalinity concentration, and (f) aragonite saturation state.

flowing into the Arctic Ocean and then Baffin Bay, a passive tracer is added along a section across Bering Strait from the beginning of the simulation that is, 1 January 2002, using the NEMO-TOP module (Aumont et al., 2018). The passive tracer concentration (C) is assigned at T points in the Arakawa C grid (Mesinger & Arakawa, 1976) along the selected section and updated every time step with an increment ΔC proportional to the volume flux at Bering Strait. Further details on the passive tracer and its implementation can be found in Hu et al. (2019). The results are presented as an idealized thickness of Pacific water present in the upper 150 m of the water column in Baffin Bay, focusing on the period 2009 to 2019. The idealized thickness of Pacific water formally represents the fraction of Pacific water in the grid cell, times the thickness of that grid cell, integrated in the vertical (in the case of this study, integrated over the upper 150 m of the water column).

4. Results and Discussion

4.1. Surface Distributions

Surface (0–5 m) distributions of calculated water mass fractions (F_{SIM} , F_{MW} , and F_{ARC}) and carbonate system parameters (DIC, TA, and Ω_{Ar}) are shown in Figure 4. The spatial distribution of these parameters strongly reflects the regional oceanography, with clear gradients between eastern and western Baffin Bay as they are influenced by the WGC and BIC, respectively. High F_{ARC} values are observed entering Baffin Bay from Nares Strait and Lancaster Sound, and flow southwards through western Baffin Bay. Surface waters with high F_{ARC} also generally coincide with low DIC, TA, and Ω_{Ar} , which is consistent with previous studies in Baffin Bay during summer, and the fact that Arctic waters are primarily composed of Pacific halocline waters (Azetsu-Scott et al., 2012; Beaupré-Laperrière et al., 2020; Shadwick et al., 2011; Yamamoto-Kawai et al., 2013). In contrast, eastern Baffin Bay (along the west Greenland shelf) displays low F_{ARC} values, since this region is dominated by Atlantic waters (F_{ATL} ; not shown) being transported northwards by the WGC (Figure 4c).

BURGERS ET AL. 9 of 21

Sea-ice melt fractions (F_{SIM}) are greatest in the western and northernmost regions where sea ice is known to persist the longest into the summer season (Bi et al., 2019; Randelhoff et al., 2019; Tang et al., 2004), although we do not observe any large SIM contributions within the study area (all F_{SIM} are below 0.1, Figure 4a). Sea-ice melt dilutes DIC and TA in surface waters (Yamamoto-Kawai et al., 2009), and indeed areas where we observe the highest F_{SIM} coincide with very low surface DIC and TA, such as Smith Sound and western Baffin Bay along the Baffin Island coastline. The relative uncertainty associated with F_{SIM} estimates was generally quite high throughout the study area (CV > 0.9), but the high positive F_{SIM} seen in Smith Sound and western Baffin Bay was apparently robust (CV < 0.5; Figure S4 in Supporting Information S1).

Significant surface meteoric water fractions (F_{MW}) are present in Lancaster Sound and Smith Sound but also show high contributions in Disko Bay and Uummannaq Fjord along the west Greenland coast (Figure 4b). Meteoric water contributions entering from Lancaster Sound and Smith Sound may be due to river runoff inputs into the central Arctic Ocean, which are now exiting through the CAA channels, or could be from small rivers within the islands of the CAA (Alkire et al., 2017; Brown et al., 2020). The fact that the F_{MW} signal in Smith Sound is not also present further north in Nares Strait may point to a nearby glacial meltwater source, such as the Trinity and Wykeham glaciers, which are currently the fastest flowing glaciers in the CAA (Dalton et al., 2019, 2022). However, we also note that the high F_{MW} signal is represented by one data point and therefore might not be robust. The highest observed F_{MW} in our study area are located in Disko Bay and Uummannaq Fjord, where many large and fast flowing tidewater glaciers expel icebergs and glacial meltwater. Disko Bay receives discharge from Sermeq Kujalleq (also known as Jakobshavn Isbræ), which has been the single largest source of mass loss from the Greenland ice sheet over the last 20 years (Mouginot et al., 2019). These large F_{MW} inputs in west Greenland fjords are also the most robust F_{MW} signal according to our Monte Carlo uncertainty analysis (Figure S4 in Supporting Information S1).

Although there is high F_{MW} entering these major west Greenland fjords, we do not observe low Ω_{Ar} at the surface (Figures 4b–4f). This is in contrast to our observations in western Baffin Bay, which display freshwater inputs mainly from Arctic waters and sea-ice melt, and have relatively low surface Ω_{Ar} . In the west Greenland fjords we observe very low surface DIC (Figure 4d), suggesting that biological uptake of CO_2 is exerting a more substantial influence on Ω_{Ar} compared to the TA decrease from glacial meltwater inputs. The west Greenland fjords and continental shelf are known to be very productive, with large spring phytoplankton blooms that strongly decrease surface DIC concentrations but do not alter TA (Burgers et al., 2020; Krawczyk et al., 2021). Due to the particularly high TA:DIC ratios in this area, these waters have a high buffering capacity against decreases in saturation state.

4.2. Varying Meteoric Water Characteristics

In order to investigate differences in meteoric water characteristics in eastern and western Baffin Bay we have plotted linear regression relationships of TA and δ^{18} O against salinity in the waters of the WGC and BIC (Figure 5). We consider measurements throughout the entire water column in these linear regression relationships. The y-intercepts of these regressions provide an estimate of freshwater end-member values for TA and δ^{18} O in these two regions of Baffin Bay. For the purpose of this investigation the BIC region shown in Figure 5 encompasses the channels of Lancaster Sound and Nares Strait, which both transport Arctic outflow waters into the BIC in western Baffin Bay. The stations near central Baffin Bay have been included in the BIC region as Arctic waters, defined as S \leq 33.3 and T < 0°C, were present in the upper water column at these locations.

It is important to consider how these linear regression relationships may be altered by the presence of sea-ice melt or formation, which have an impact on salinity, TA, and δ^{18} O properties. Here, we perform a correction on salinity and TA to account for sea-ice related processes following the method of Yamamoto-Kawai et al. (2005):

$$S_0 = (S - S_{SIM} F_{SIM}) / (1 - F_{SIM})$$
(10)

$$TA_0 = (TA - TA_{SIM} F_{SIM}) / (1 - F_{SIM})$$
 (11)

where S_0 and TA_0 are salinity and TA corrected for the influence of sea-ice melt or formation. Values of F_{SIM} were calculated previously for each sample using salinity and $\delta^{18}O$ observations in Equations 5–7. We apply a value of 420 μ mol kg⁻¹ for TA_{SIM} (Miller et al., 2011; Rysgaard et al., 2007) and 4 for S_{SIM} (Table 2). We are

BURGERS ET AL. 10 of 21

21699291, 2024, 8, Downloaded from https://agupubs.onlinelibrary.wiley.com/doi/10.1029/2024JC021122 by Kathkem Mary Stafford - Oregon State University, Wiley Online Library on [29/07/2025], See the Terms and Conditions (https://onlinelibrary.wiley.

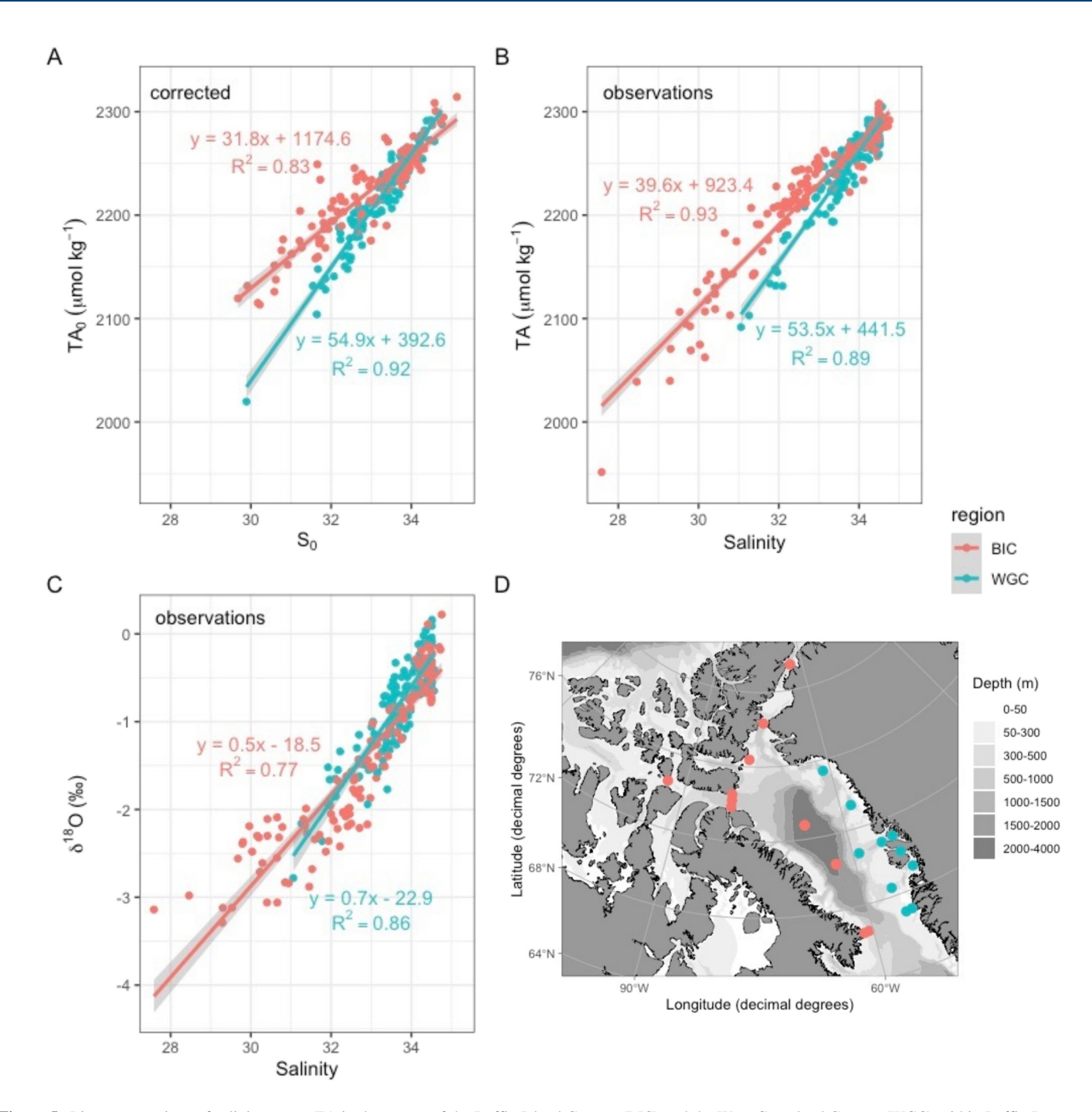


Figure 5. Linear regressions of salinity versus TA in the waters of the Baffin Island Current (BIC) and the West Greenland Current (WGC) within Baffin Bay, (a) corrected values (Equations 10 and 11) for the influence of sea-ice melt or formation, (b) observed salinity-TA relationships, (c) observed salinity- δ^{18} O relationships, (d) map showing station locations for the BIC region (red) and WGC region (blue) used to determine the regression relationships in panels (a) through (c).

unable to perform a similar sea-ice process correction to the $\delta^{18}O$ values, since we have already used these measurements to calculate the F_{SIM} estimates used in the correction. Performing the correction would simply reinforce our chosen meteoric water $\delta^{18}O$ end-member value of -20%.

Based on the resulting linear regressions, the waters of the WGC display a much lower freshwater TA endmember (*y*-intercept) compared to the BIC in western Baffin Bay. For waters of the WGC, the *y*-intercept of the observed salinity-TA plot (Figure 5b) is $440 \pm 150 \, \mu \text{mol kg}^{-1}$, whereas for waters of the BIC the *y*-intercept of the observed salinity-TA relationship is $920 \pm 76 \, \mu \text{mol kg}^{-1}$ (note that all stated uncertainty values are based on

BURGERS ET AL. 11 of 21

the 99% confidence levels of the regression relationships). This already suggests that there is quite a large difference between the estimated meteoric TA end-member values of eastern and western Baffin Bay. After applying corrections for the impacts of sea-ice melt or formation (Figure 5a), the *y*-intercept of the salinity-TA relationships become 390 \pm 140 μ mol kg⁻¹ for the WGC, and 1,170 \pm 120 μ mol kg⁻¹ for the BIC, further enhancing the difference in estimated meteoric TA end-member values between these two regions of Baffin Bay. It is interesting to note that the intersection points of the observed and corrected salinity-TA regressions change from being located at a salinity of 34.7 to 33.8, respectively. This presumably indicates that in the absence of sea ice related processes (melt or brine inputs) the water mass salinity and TA properties would be the same at a salinity of approximately 33.8 in both the WGC and BIC regions. Estimates of δ^{18} O meteoric end-member values using the observed salinity- δ^{18} O relationships show *y*-intercept values of $-23 \pm 3.0\%$ for the WGC, and $-18 \pm 1.4\%$ for the BIC (Figure 5c). These are relatively similar meteoric δ^{18} O end-member values in both regions, but applying an analysis of covariance (ANCOVA) by region found the slopes and *y*-intercepts of the WGC and BIC regression relationships for salinity- δ^{18} O to be statistically different (*p*-value <0.05).

The corrected meteoric TA end-member for the BIC region $(1,170 \pm 120 \,\mu\text{mol kg}^{-1}; \text{Figure 5a})$ agrees quite well with previous estimates of TA in average river runoff into the Arctic Ocean (e.g., $831 \pm 100 \,\mu\text{mol kg}^{-1}$ from Yamamoto-Kawai et al., 2005; flow-weighted average of 1,048 $\,\mu$ mol kg⁻¹ from Cooper et al., 2008; $1,000 \pm 100 \,\mu\text{mol kg}^{-1}$ in the Transpolar drift stream from Charette et al., 2020). This would be consistent with the BIC region receiving Arctic outflow waters and transporting them southwards along the Baffin Island shelf and slope into the Labrador Sea.

We hypothesize that the much lower TA end-member found in the WGC region $(390 \pm 140 \, \mu \text{mol kg}^{-1}; \text{Figure 5a})$ indicates that glacial meltwater is the dominant source of fresh water on the west Greenland shelf. TA measurements of glacial discharge across the Arctic have so far revealed a range from 20 to 550 µmol kg⁻¹ (Henson et al., 2023; Hopwood et al., 2020; Rysgaard et al., 2012), which spans our calculated TA end-member value for the WGC region. The type of bedrock below a glacier can also greatly affect the TA end-member of its meltwater (Azetsu-Scott et al., 2014; Fransson et al., 2015). If calcareous bedrock, such as limestone or marble, is present, it would be expected to increase the TA end-member of the meltwater by contributing bicarbonate or carbonate ions from weathering. Geological maps available from the Geological Survey of Denmark and Greenland (GEUS) through their Greenland Portal indicate that the bedrock along the west Greenland coast is predominantly composed of orthogneiss all the way from Kangerlussaq in the south (approximately 67°N) to the Nussuaq Peninsula in the north (approximately 74°N) (Escher, 1985; Garde & Marker, 2010). Orthogneiss is formed by the metamorphism of igneous rocks, is not calcareous, and therefore would not be expected to contribute any additional TA to glacial meltwater, consistent with the low TA freshwater end-member value we have derived for this region. The highly depleted δ^{18} O meteoric end-member found in the WGC $(-23 \pm 3\%)$ may also be consistent with a significant contribution of glacial meltwater. Carlson et al. (2019) collected glacial ice samples from icebergs in Nuup Kangerlua (Godthåbsfjord), in early January 2019 using an ice drone, and found the icebergs to have a mean δ^{18} O value of $-26.33 \pm 0.08\%$. Since our linear regressions in Baffin Bay do not include measurements of water with very low salinities, and the v-intercepts are therefore interpolations, we cannot state conclusively that glacial meltwater is the main source of meteoric waters on the west Greenland shelf, although we surmise this is likely the case, seeing as the central west Greenland coastline houses many large and fastflowing tidewater glaciers (Mouginot et al., 2019), coupled with the large difference in TA meteoric endmember values we derived for the WGC and BIC.

4.3. The West Greenland Shelf

The waters of the west Greenland shelf have been relatively understudied compared to the BIC in western Baffin Bay. Figure 6 shows the physico-chemical characteristics of the water column from Davis Strait in the south to Melville Bay in the north (including an eastward diversion into Disko Bay). Near the surface we observe a shallow fresh and warm layer that has been heated by solar insolation (Figure 6a). This layer contains relatively high fractions of meteoric waters which appear in Disko Bay and Uummannaq Fjord (Figure 6d) and are transported northwards with the WGC. Between depths of 40–150 m there is a temperature minimum layer centered at a salinity of approximately 33.5, representing BBPW (Figures 6a and 6b). The coldest temperatures of the BBPW layer are observed at the northern end of the west Greenland shelf, suggesting that its formation site is located

BURGERS ET AL. 12 of 21

21699291, 2024, 8, Downloaded from https://agupubs.onlinelibrary.wiley.com/doi/10.1029/2024JC021122 by Kathleen Mary Stafford - Oregon State University, Wiley Online Library on [29/07/2025]. See the Terms and Conditions (https://onlinelibrary.wiley.

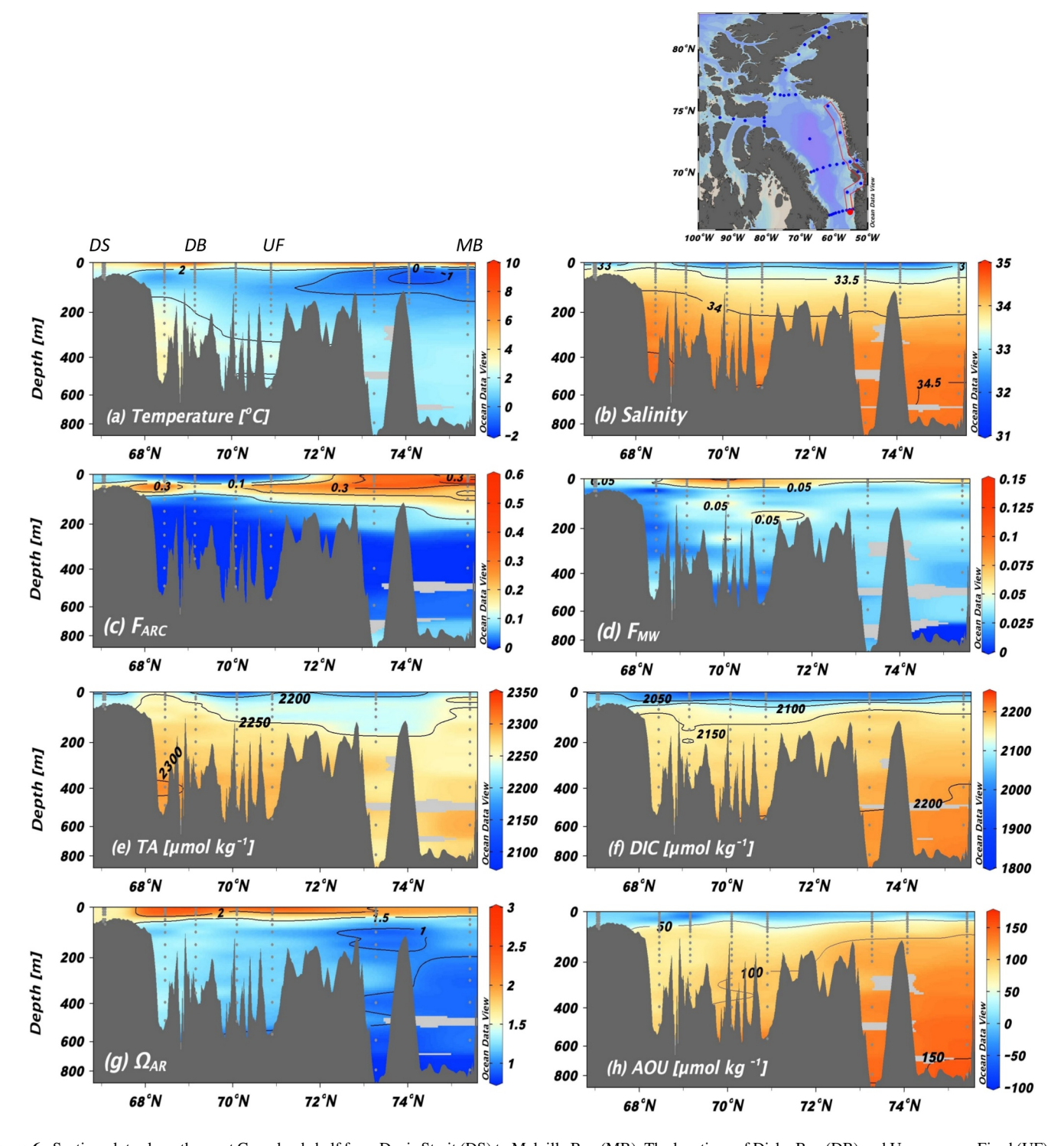


Figure 6. Section plots along the west Greenland shelf from Davis Strait (DS) to Melville Bay (MB). The locations of Disko Bay (DB) and Uummannaq Fjord (UF) are shown along the top of panel (a), and the transect location is outlined in red in the top-right map. Section plots show spatial distributions of various physico-chemical properties: (a) Temperature, (b) Salinity, (c) the fraction of Arctic water (F_{ARC}), (d) the fraction of meteoric water (F_{MW}), (e) total alkalinity (TA), (f) dissolved inorganic carbon (DIC), (g) aragonite saturation state (Ω_{Ar}), and (h) apparent oxygen utilization (AOU).

somewhere in northern Baffin Bay. The deepest water mass on the west Greenland shelf is the relatively warm and saline SPMW, which can be seen entering from the south and shows a decreasing temperature maximum toward the north (Figure 6a).

BURGERS ET AL. 13 of 21

We find significant F_{ARC} within the upper 150 m of the West Greenland shelf transect, especially in the northernmost half of the transect (Figure 6c). The highest F_{ARC} value of the transect (0.57) is found at 30 m depth at the northernmost station. Along the rest of the transect, maximum F_{ARC} ranges between 0.15 and 0.4 and is generally found at depths of 60 or 70 m, coinciding with the coldest temperatures of the BBPW layer with salinity values between 33.4 and 33.6 (Figures 6a and 6b). It is surprising to see relatively high F_{ARC} on the west Greenland shelf, since Arctic waters are thought to flow predominantly southwards along the Baffin Island shelf and slope with the BIC. Since our F_{ARC} values are calculated based on DIN:P ratios (see Figure 3 and Section 3.3), it is possible that local denitrification could alter the DIN:P ratio, leading to a false identification of Arcticoutflow waters. If denitrification were the cause of these relatively high F_{ARC} values on the West Greenland shelf, it would likely originate from the very productive and shallow continental shelves in southeastern Baffin Bay (near Disko Bay and further south). Using the few stations in this data set over the continental shelf in southeastern Baffin Bay, we investigated whether there was any signal of benthic denitrification that could be leading to falsely high F_{ARC} values, but found no evidence of denitrification (see Figure S6 in Supporting Information S1). In fact, we found higher dissolved oxygen concentrations, lower AOU, and lower DIC over the shallow continental shelf compared to waters offshore of the shelf break. If there were local denitrification occurring in this area, we would expect these trends to be reversed. Therefore, we do not anticipate that local denitrification is responsible for the relatively high F_{ARC} values we derived over the West Greenland shelf, and we expect that the F_{ARC} values are in fact due to the transport of Arctic-outflow waters to this region.

The presence of significant FARC in the BBPW layer suggests that this water mass may be formed in an area where surface waters contain some portion of Arctic-outflow waters. Such an area might be the North Water polynya region in northern Baffin Bay, which receives Arctic waters from the outflow of Nares Strait, and also receives comparatively more saline surface waters from the WGC. It is possible that winter convection mixes surface water contributions from both the BIC and WGC, leading to the formation of BBPW at an intermediate salinity. However, our observations show that BBPW displays lower TA concentrations compared to what would be expected from Arctic-outflow waters at the same salinity by roughly 20 µmol kg⁻¹ (based on the observed TA vs. salinity regressions in Figure 5b). The reason for this is unclear. One hypothesis could be that glacial meltwater is also incorporated into BBPW during its formation in winter. Another hypothesis could be the explusion of relatively low-TA brine during sea-ice formation, with TA being retained in the sea ice as ikaite crystals (Papadimitriou et al., 2007; Rysgaard et al., 2007). More research is needed into the location and formation mechanisms of BBPW in order to fully comprehend the TA characteristics of this water mass. Our observations also show a zone of undersaturated Ω_{Ar} near the bottom of the BBPW layer at approximately 73°N (Figure 6g), due to the relatively low TA:DIC ratio at this location (at this depth DIC has not been lowered by surface primary production). This is notable since previously reported values of Ω_{Ar} in BBPW have not noted any undersaturation (AMAP, 2018).

Below 200 m, the water column is mainly composed of SPMW, which upon entering Baffin Bay in the south contains high TA (average of 2,280 \pm 10 μ mol kg⁻¹; Figure 6e) and moderate DIC (average of 2,160 \pm 10 μ mol kg⁻¹; Figure 6f). As the SPMW flows northwards, its TA decreases and DIC increases, decreasing Ω_{Ar} . Increasing DIC at depths below 200 m coincides with increasing Apparent Oxygen Utilization (AOU; Figure 6h), which represents the deviation from O_2 saturation. This suggests the respiration of organic matter is responsible for the increases in DIC at these depths. TA also decreases slightly with organic matter respiration, although in this case respiration cannot account for the total observed decrease in TA. The average TA value in the Melville Bay region decreased to 2,268 \pm 5 μ mol kg⁻¹, representing an average decrease of 12 μ mol kg⁻¹ from the SPMW entering Baffin Bay at eastern Davis Strait. Assuming traditional Redfield ratios (6 DIN: 106 DIC), organic matter respiration would account for approximately 2 μ mol kg⁻¹ of this TA decrease. The reason for the additional TA decrease at depth is uncertain.

4.4. The Eastward Propogation of Arctic Waters

The presence of Arctic waters on the west Greenland shelf suggests that there is a significant west-to-east flow across Baffin Bay. There is limited observational support for this notion, due to the relatively small number of studies relating to the physical oceanography of Baffin Bay. Myers and Ribergaard (2013) observed cold and relatively fresh Arctic waters in Disko Bay prior to 1997, but post-1997 this layer, located at depths between 30 and 200 m, warmed by 1–2°C. The authors suggested that this disappearance of the Arctic water layer in Disko Bay was related to circulation changes in Baffin Bay, and supported this using regional ocean modeling results

BURGERS ET AL. 14 of 21

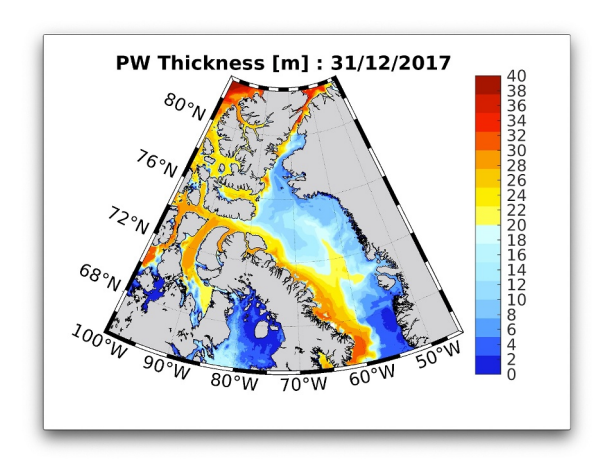


Figure 7. Snapshot of the Pacific water thickness throughout the upper 150 m of Baffin Bay, in meters, based upon a passive tracer in a 1/12° NEMO model simulation of the Arctic and North Atlantic. Pacific water thickness values are calculated as the fraction of the Pacific water tracer, times the thickness of the grid cell, integrated in the vertical (in this case over the upper 150 m of the water column). The figure shows a snapshot of the 5 days average ending on 31 December 2017, to show an example of an instance where a pulse of Pacific waters is propagated eastwards from the Baffin Island Current into central Baffin Bay, and ultimately onto the west Greenland shelf.

that looked at conservation of vorticity and flow following lines of f/H (where f is the Coriolis parameter and H is the depth). Azetsu-Scott et al. (2012) also noted a sub-surface extension of Arctic waters propagating eastwards at Davis Strait, forced by a combination of the bottom topography along the western margin of Davis Strait and the tendency of currents to follow f/H contours. At the time of our observations in 2019, some F_{ARC} was present in a narrow layer between 30 and 80 m in Disko Bay (Figure 6c), although we observed a much larger volume of Arctic waters toward the north, in Melville Bay (from the surface to 150 m depth).

Following on the modeling study of Wu et al. (2012), which examined circulation patterns in the upper water column (depths <200 m) and showed an extension of the BIC toward the center of Baffin Bay, we use a passive tracer, run online as part of a high resolution numerical model simulation, to assess the circulation of Pacific-source Arctic waters in Baffin Bay (Section 3.4). The model simulation correctly shows the entrance of Pacific water into Baffin Bay from the passages of the CAA and its predominant southward flow along the Baffin Island shelf and slope. At certain times, the simulation shows a pulse of Pacific water moving eastwards, toward the west Greenland shelf (such an instance is shown in Figure 7). A full movie of the passive tracer simulation is provided by Myers (2023). Instances when the model simulation shows an eastward propagation of Pacific waters were found to coincide with a change in wind direction and associated Ekman transports. Most of the year the Ekman transport in western Baffin Bay is directed onshore constraining Pacific waters on the Baffin Island shelf. When the wind direction reverses,

Ekman transport is then offshore, toward the center of the bay, and ultimately over onto the west Greenland shelf. At the end of the passive tracer simulation, the highest Pacific water tracer concentrations over the west Greenland shelf were centered at approximately 40 m depth (± 10 m), with Pacific water fractions greater than 0.1 being present at depths between 10 and 130 m depending on the location. This aligns fairly well with the depths of our highest calculated F_{ARC} values from observations along the West Greenland shelf, which ranged from being more shallow in the north (30 m) to deeper in the south (60–70 m) of the transect (Figure 6c).

4.5. Bay-Wide Drivers of Ω_{Ar}

We now consider a bay-wide perspective of Ω_{Ar} values to examine the main biogeochemical processes controlling its distribution. Figure 8a shows Ω_{Ar} values plotted in DIC-TA space. Generally, low values of TA and DIC are located in the upper water column, and high values at depth. Two main trends can be seen in Ω_{Ar} . First, an east-west trend can be seen with relatively high Ω_{Ar} values located in the surface waters of the major fjord systems of central west Greenland, and relatively low Ω_{Ar} values located in the surface water of the BIC in western Baffin Bay (also seen in Figure 4f). Second, we observe a trend in Ω_{Ar} with depth, with deeper waters generally displaying lower Ω_{Ar} values (Figures 6g and 8a). The most undersaturated Ω_{Ar} values were observed in BBDW and BBBW (0.36–0.59), with other undersaturated Ω_{Ar} values (Ω_{Ar} < 1) observed in the SPMW (Atlantic) layer. The primary drivers of these two trends are evident from Figures 8b and 8c.

Different processes and factors affect Ω_{Ar} at different depths in the water column. Figure 8b isolates measurements from the upper 200 m of the water column and displays F_{ARC} values in DIC-TA space. In these shallower waters of Baffin Bay there is a strong east-west divide in water masses, because of the presence of the WGC in eastern Baffin Bay, and the BIC to the west. Due to the fact that Arctic waters in the BIC are primarily composed of relatively low salinity Pacific waters, and additional freshwater inputs from sea-ice melt and meteoric waters, they are characterized by a relatively low TA to DIC ratio. This drives lower Ω_{Ar} values in the upper water column of the BIC. In contrast, the upper water column of the WGC is mainly composed of Atlantic waters, with a relatively high TA to DIC ratio and therefore higher Ω_{Ar} . Near surface waters in the major fjord systems of western Greenland displayed the highest Ω_{Ar} values (Figure 6g), likely due to strong primary production in this region (Burgers et al., 2020; Jensen et al., 1999; Krawczyk et al., 2021), which lowers DIC without significantly affecting TA.

BURGERS ET AL. 15 of 21

onlinelibrary.wiley.com/doi/10.1029/2024JC021122 by Kathleen Mary Stafford - Oregon State

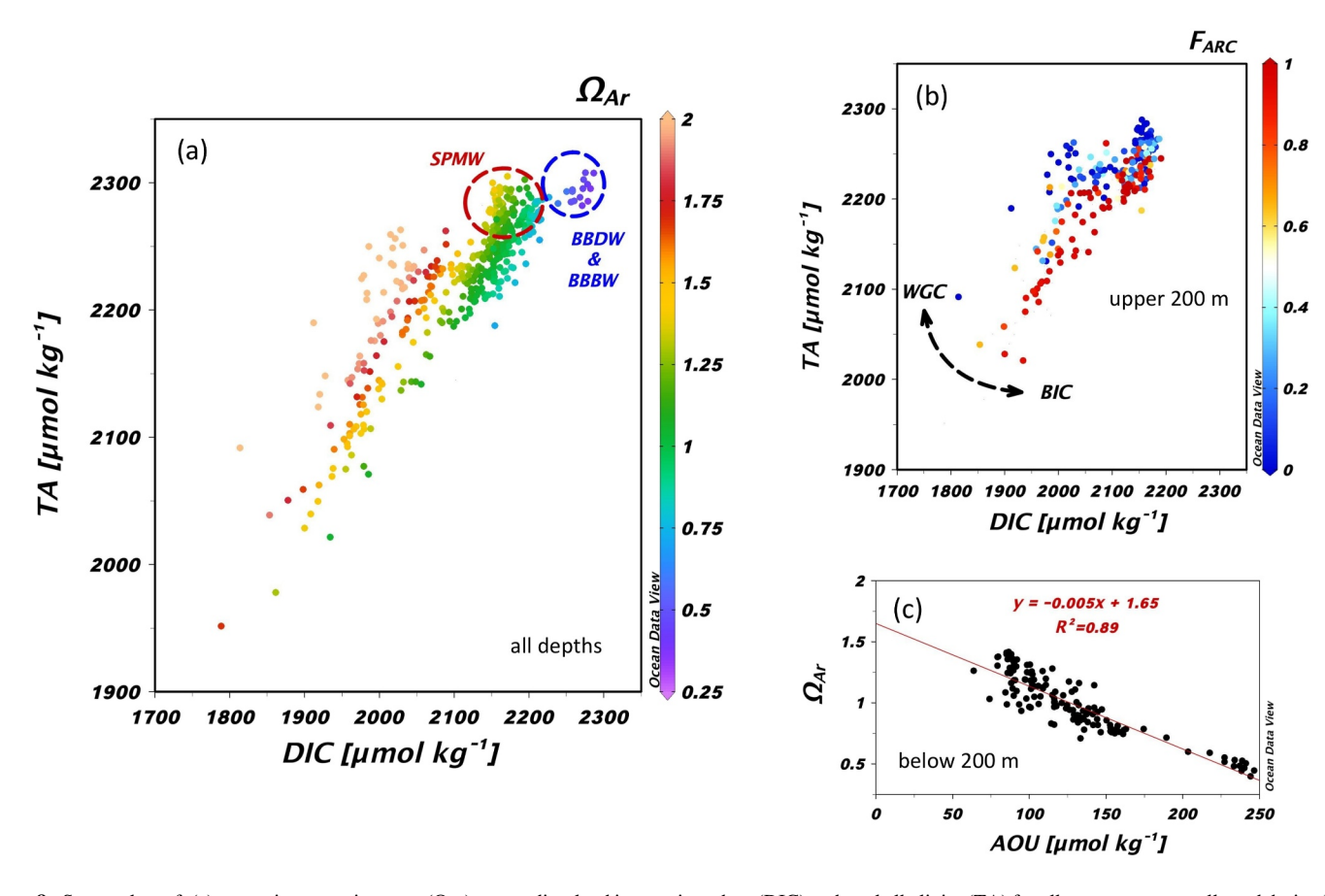


Figure 8. Scatterplots of: (a) aragonite saturation state (Ω_{Ar}) versus dissolved inorganic carbon (DIC) and total alkalinity (TA) for all measurements collected during Leg 2 of the 2019 Amundsen expedition; (b) fraction of Arctic water (F_{ARC}) versus DIC and TA for all measurements in the upper 200 m of the water column; and (c) apparent oxygen utilization (AOU) versus Ω_{Ar} for all measurements below 200 m depth. The red circle in (a) indicates subpolar mode water (SPMW), and the blue circle represents Baffin Bay Deep Water (BBDW) and Baffin Bay Bottom Water (BBBW). Dashed arrows in (b) show how measurements in the upper water column are distributed spatially between the WGC and BIC across Baffin Bay.

Below 200 m, SPMW dominates the mid-water column in both western and eastern Baffin Bay. The only other water masses present below 200 m are BBDW and BBBW, which are located below 1,200 m in the deep central basin of Baffin Bay. We do not observe large variations in TA at depths below 200 m, but we do see a large gradient in DIC (Figure 8a). This is consistent with the respiration of organic matter, which releases DIC into the surrounding waters and consumes oxygen (leading to increases in AOU) with minimal changes to TA. Figure 8c reinforces the point that organic matter respiration is the main driver of Ω_{Ar} variations below 200 m, by showing a strong negative correlation between AOU and Ω_{Ar} in these waters. The most undersaturated values of Ω_{Ar} are present in BBDW and BBBW, waters with a very long residence time (hundreds of years; Zeidan et al., 2022) and consequent accumulation of respiratory DIC. Within the SPMW layer the lowest Ω_{Ar} and highest AOU are located in western Davis Strait where this water mass exits Baffin Bay after its full counter-clockwise circulation.

4.6. Temporal Changes in Ω_{Ar} Across Davis Strait

Here we examine temporal changes in the distribution of Ω_{Ar} across Davis Strait by comparing measurements (including temperature and salinity) from 1997, 2004 and 2019 (Figure 9). We refer to measurements taken in 1997 and 2004 as "historical" data. Measurements across Davis Strait were used for this temporal analysis because it was the only location in Baffin Bay where multiple stations were sampled at an approximately consistent location between our 2019 data set and historical ones.

Year-to-year variability in the distribution of Arctic waters and SPMW across Davis Strait heavily influences the distribution of Ω_{Ar} . The Ω_{Ar} saturation horizon shoaled between 2004 and 2019, with $\Omega_{Ar} < 1$ present in western Davis Strait at depths between 50 and 200 m in 2019. If these undersaturated waters reach the Baffin Island shelf

BURGERS ET AL. 16 of 21

from https://agupubs.onlinelibrary.wiley.com/doi/10.1029/2024JC021122 by Kathleen Mary Stafford - Oregon State University

, Wiley Online Library on [29/07/2025]. See the Term

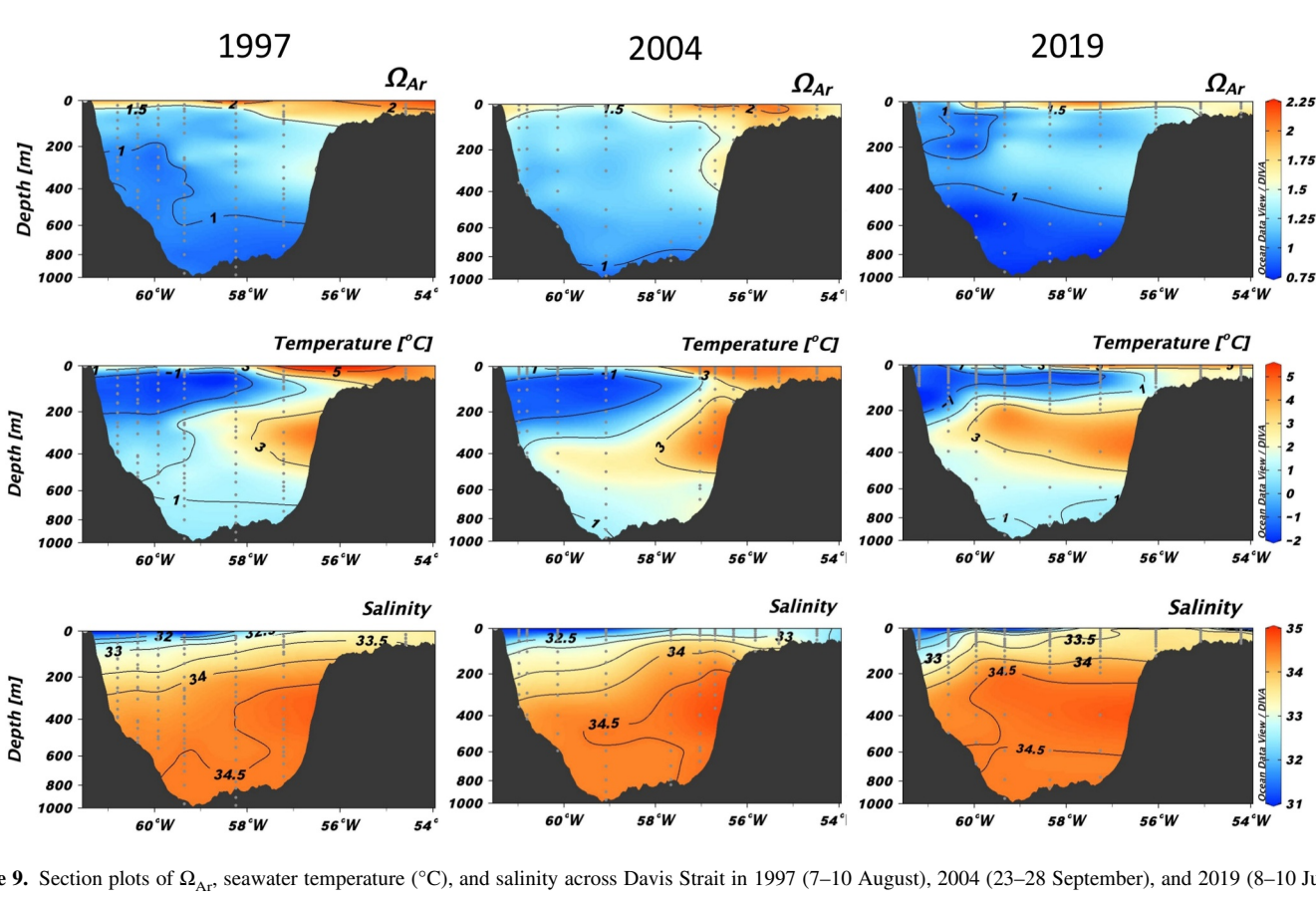


Figure 9. Section plots of Ω_{Ar} , seawater temperature (°C), and salinity across Davis Strait in 1997 (7–10 August), 2004 (23–28 September), and 2019 (8–10 July).

ecosystem, they could pose a potential threat to calcifying organisms. We observe a statistically significant decrease in Ω_{Ar} of Arctic waters between the historical data and those from 2019, according to unpaired t-tests (pvalues <0.001; Table 3), which coincides with a significant decrease in TA (unpaired t-test, p-value <0.001) but no significant change in DIC or salinity. A typical mechanism that would lead to decreasing TA would be freshwater inputs, but this would also coincide with observable decreases in salinity. The average salinity of Arctic waters in 2019 did decrease compared to 1997 and 2004, but the change was not statistically significant (Table 3). Further studies are required with more data points to determine what is driving decreases in Ω_{Ar} in Arctic waters, and if the trend of decreasing TA we have identified is indeed real over a longer timeseries. We do not observe significant Ω_{Ar} decreases between years for any other water mass present in the Davis Strait transect (Table 3). Having measurements spanning two decades, we expected that perhaps an increase in DIC due to increased uptake of atmospheric CO2 would be present in this temporal analysis, but we did not observe any significant signal of this, in any water mass. Since the physical oceanography of the region is so variable, this likely precludes us from being able to identify an anthropogenic signal, yet.

Although it is not a statistically significant trend, the SPMW layer in Davis Strait also displays a lower mean Ω_{Ar} in 2019 compared to 1997 and 2004 (Table 3). The lowest Ω_{Ar} values seen in the SPMW layer each year generally coincide with the relatively cold version of SPMW that exits Baffin Bay at Davis Strait (with approximate properties of $T < 2^{\circ}C$ and S > 34.3). These low saturation states result from physical and biochemical changes to SPMW along its cyclonic flow path around Baffin Bay. SPMW is significantly cooled as it transits north along the west Greenland shelf, and shows a slight decrease in TA from south to north. Additionally, this water mass accumulates DIC from the respiration of organic matter along its flow path (as indicated in Figure 6). These processes combined contribute to lowering the Ω_{Ar} of SPMW along its flow path, leading to a gradient in Ω_{Ar} within the SPMW layer across Davis Strait (where SPMW both enters and exits Baffin Bay). This reinforces the trend of decreasing Ω_{Ar} in SPMW that we observed from south to north on the west Greenland shelf, and shows that these waters continue to accumulate respiration products as they are redirected southwards back toward Davis Strait, with the BIC.

BURGERS ET AL. 17 of 21

Table 3Water Mass Properties (Mean \pm SD) Across Davis Strait in 1997, 2004, and 2019, With the Number of Observations (n) Averaged for Each Water Mass Indicated in Parentheses

Measure	Year	ARC	BBPW	SPMW
$\Omega_{ m Ar}$	1997	$1.20 \pm 0.05 $ (17)	$1.06 \pm 0.08 (10)$	1.05 ± 0.15 (40)
	2004	1.31 ± 0.08 (8)	1.27 ± 0.06 (6)	$1.23 \pm 0.22 (18)$
	2019	$1.02 \pm 0.04 (19)$	1.10 ± 0.14 (6)	0.97 ± 0.18 (20)
TA	1997	$2,242 \pm 7 (18)$	$2,246 \pm 9 \ (10)$	$2,276 \pm 11 (42)$
	2004	$2,242 \pm 11 \ (8)$	$2,258 \pm 11$ (6)	$2,288 \pm 14 (18)$
	2019	$2,208 \pm 17 (19)$	$2,223 \pm 7 (6)$	$2,264 \pm 13 (20)$
DIC	1997	$2,137 \pm 9 (17)$	$2,157 \pm 15 (10)$	$2,183 \pm 19 (40)$
	2004	$2,124 \pm 19 (8)$	$2,139 \pm 5 (6)$	$2,171 \pm 27 (20)$
	2019	$2,127 \pm 20 (19)$	$2,132 \pm 19$ (6)	$2,185 \pm 21 \ (20)$
Salinity	1997	$33.0 \pm 0.2 (24)$	$33.5 \pm 0.1 (10)$	$34.4 \pm 0.2 (44)$
	2004	$32.8 \pm 0.3 (15)$	$33.5 \pm 0.1 (10)$	$34.4 \pm 0.2 (30)$
	2019	$32.6 \pm 0.4 (55)$	$33.5 \pm 0.1 (19)$	34.4 ± 0.2 (21)

Note. Arctic water (ARC), Baffin Bay Polar water (BBPW), Sub-polar mode water (SPMW).

We also investigated inter-annual changes in carbon system variables in BBDW and BBBW, using cruise data that accessed the deep central basin of Baffin Bay in 1997 and 2003, as well as our 2019 data (see Figure S7 in Supporting Information S1 for the historical station locations). We find no significant changes in Ω_{Ar} , DIC, TA and pH between years (see Table S1 in Supporting Information S1).

5. Summary and Conclusions

This work provides an updated analysis of the main biogeochemical drivers influencing trends in $\Omega_{\rm Ar}$ throughout Baffin Bay. Spatially, we find that different processes are important in different regions, and at different depths in the bay. Within the upper 200 m, increasing $F_{\rm ARC}$ is the primary driver of decreasing $\Omega_{\rm Ar}$, due to the low TA:DIC ratio of Arctic-outflow waters. At depths below 200 m, respiration of organic matter is the main driver of low $\Omega_{\rm Ar}$. Within the SPMW layer, the amount of respiration tends to increase along the cyclonic flow path of this water mass around Baffin Bay. To examine temporal trends in $\Omega_{\rm Ar}$, we compared "historical" measurements across Davis Strait from the years 1997 and 2004 with our 2019 data set. We observe a statistically significant decrease in the $\Omega_{\rm Ar}$ of Arctic waters between the historical years and 2019, coinciding with a significant decrease in TA, but no significant changes in DIC or salinity. No other water masses across Davis Strait displayed any significant temporal changes in $\Omega_{\rm Ar}$, TA, DIC or

salinity. It is likely that the large variability in the physical oceanography of this region precludes us from identifying any anthropogenic ocean acidification signal at this time.

We observe significant F_{ARC} within the BBPW layer on the northern portion of the west Greenland shelf, coinciding with decreases in TA and Ω_{Ar} . Using a passive tracer included in a numerical modeling simulation, we find that periodic changes in wind direction lead to a switch from onshore to offshore Ekman transport in western Baffin Bay, transporting Arctic waters toward central Baffin Bay and ultimately onto the west Greenland shelf. This goes against the conventional view of a persistent cyclonic circulation in Baffin Bay and suggests there is still much to be learned about the physical oceanography of Baffin Bay, its seasonal and interannual variability and how it may be changing.

Freshwater inputs in western Baffin Bay, which result from a combination of Pacific-source halocline waters, seaice melt, and meteoric waters, are associated with lower Ω_{Ar} than the freshwater inputs in eastern Baffin Bay, which are assumed to primarily originate from glacial meltwater. Based on salinity-TA linear regression relationships (corrected for the influences of sea-ice related processes; Figure 5a), surface waters on the west Greenland shelf have a significantly lower meteoric end-member TA value (390 \pm 140 μ mol kg⁻¹) compared to surface waters of the BIC in western Baffin Bay (1,170 \pm 120 μ mol kg⁻¹). In contrast, the difference between the δ^{18} O meteoric end-members of these two regions is relatively small. The low TA freshwater end-member we have derived here agrees well with the limited measurements of glacial meltwater TA that have been reported in recent literature (Hopwood et al., 2020; Meire et al., 2015; Rysgaard et al., 2012).

Data Availability Statement

Seawater measurements of temperature, salinity, and dissolved oxygen concentrations presented herein were made available by the Amundsen Science program (Amundsen Science Data Collection, 2024), which was supported by the Canada Foundation for Innovation and Natural Sciences and Engineering Research Council of Canada. The views expressed in this publication do not necessarily represent the views of Amundsen Science or that of its partners. The full seawater geochemical data set from Leg 2 of the 2019 Amundsen scientific expedition is available through OCADS at NCEI accession 0290861 (Burgers et al., 2024). Historical data sets of seawater carbonate system parameters are available on GLODAPv2.2022 (Lauvset et al., 2022). Measurements from cruises in 1997, 2003 and 2004 were accessed using expocodes 18SN19970803, 32H120030721, and 316N20040922, respectively.

BURGERS ET AL. 18 of 21

Acknowledgments

Thanks to the captain and crew of the CCGS Amundsen, as well as Anissa Merzouk and Alexandre Forest for logistical support. We are especially thankful to Sarah Prestie, Shawn Marriott, and Cara Manning for conducting the sample collection for salinity, DIC/TA and δ^{18} O; Mohamed Ahmed for assistance with field planning and the δ^{18} O analyses; Stephen Punshon, Marty Davelar and Danielle Caleb for logistical assistance and DIC/TA analyses; Jonathan Gagnon and Gabrielle Deslongchamps for nutrient sample collection and analysis; and the Amundsen Science technicians for the collection and processing of the CTD data. A special thank you to Karen Alley and Kristina Brown for assistance interpreting geological maps of west Greenland and for many helpful discussions. Financial support for this work was provided by ArcticNet, NSERC's Canada Postgraduate Scholarships Doctoral (PGS-D) and Discovery Grant programs, the Aquatic Climate Change Adaptation Services Program (ACCASP) of Fisheries and Oceans Canada, and by the CERC program at the University of Manitoba (D. Dahl-Jensen). Financial support for the historical data sets used in this work came from the Davis Strait Observing System, which is funded by Fisheries and Oceans Canada (OFSI) and the U.S. National Science Foundation (ARC0632231).

References

- Alkire, M. B., Jacobson, A. D., Lehn, G. O., Macdonald, R. W., & Rossi, M. W. (2017). On the geochemical heterogeneity of rivers draining into the straits and channels of the Canadian Arctic Archipelago. *Journal of Geophysical Research: Biogeosciences*, 122(10), 2527–2547. https://doi.org/10.1002/2016JG003723
- AMAP. (2013). AMAP assessment 2013: Arctic cidification. Arctic Monitoring and Assessment Programme (AMAP).
- AMAP. (2018). AMAP assessment 2018: Arctic ocean acidification. Arctic Monitoring and Assessment Programme (AMAP).
- Amundsen Science Data Collection. (2024). CTD data collected by the CCGS Amundsen in the Canadian Arctic. ArcticNet Inc., Québec, Canada. Processed data. Cruise 1902 Release 1. Canadian Cryospheric Information Network (CCIN). https://doi.org/10.5884/12713
- Aumont, O., Éthé, C., Lovato, T., Mouchet, A., Nurser, G., Palmiéri, J., et al. (2018). Tracers in Ocean Paradigm (TOP) The NEMO passive Tracers engine. Zenodo. Notes du Pôle de modélisation de l'Institut Pierre-Simon Laplace (IPSL) (v4.2.0, Number 28). https://doi.org/10.5281/zenodo.1471700
- Azetsu-Scott, K., Clarke, A., Falkner, K., Hamilton, J., Jones, E. P., Lee, C., et al. (2010). Calcium carbonate saturation states in the waters of the Canadian Arctic Archipelago and the Labrador Sea. *Journal of Geophysical Research*, 115(C11), C11021. https://doi.org/10.1029/2009JC005917
- Azetsu-Scott, K., Petrie, B., Yeats, P., & Lee, C. (2012). Composition and fluxes of freshwater through Davis Strait using multiple chemical tracers. *Journal of Geophysical Research*, 117(C12). C12011. https://doi.org/10.1029/2012JC008172
- Azetsu-Scott, K., Starr, M., Mei, Z.-P., & Granskog, M. (2014). Low calcium carbonate saturation state in an Arctic inland sea having large and varying fluvial inputs: The Hudson Bay system. *Journal of Geophysical Research: Oceans*, 119(9), 6210–6220. https://doi.org/10.1002/2014JC009948
- Bâcle, J., Carmack, E. C., & Ingram, R. G. (2002). Water column structure and circulation under the north water during spring transition: April-July 1998. Deep-Sea Research Part II Topical Studies in Oceanography, 49(22–23), 4907–4925. https://doi.org/10.1016/S0967-0645(02) 00170-4
- Ballinger, T. J., Moore, G. W. K., Garcia-Quintana, Y., Myers, P. G., Imrit, A. A., Topál, D., & Meier, W. N. (2022). Abrupt northern Baffin Bay autumn warming and sea-ice loss since the turn of the twenty-first century. *Geophysical Research Letters*, 49(21), e2022GL101472. https://doi.org/10.1029/2022GL101472
- Bamber, J. L., Tedstone, A. J., King, M. D., Howat, I. M., Enderlin, E. M., van der Broeke, M. R., & Noel, B. (2018). Land ice freshwater budget of the Arctic and North Atlantic Oceans: 1. Data, methods and results. *Journal of Geophysical Research: Oceans*, 123(3), 1827–1837. https://doi.org/10.1002/2017JC013605
- Barnier, B., Madec, G., Penduff, T., Molines, J.-M., Treguier, A.-M., Le Sommer, J., et al. (2006). Impact of partial steps and momentum advection schemes in a global ocean circulation model at eddy-permitting resolution. *Ocean Dynamics*, 56(5–6), 543–567. https://doi.org/10.1007/s10236-006-0082-1
- Beaupré-Laperrière, A., Mucci, A., & Thomas, H. (2020). The recent state and variability of the carbonate system of the Canadian Arctic Archipelago and adjacent basins in the context of ocean acidification. *Biogeosciences*, 17(14), 3923–3942. https://doi.org/10.5194/bg-17-3923-2020
- Bi, H., Zhang, Z., Wang, Y., Xu, X., Liang, Y., Huang, J., et al. (2019). Baffin Bay sea ice inflow and outflow: 1978-1979 to 2016-2017. *The Cryosphere*, 13(3), 1025–1042. https://doi.org/10.5194/tc-13-1025-2019
- Bouillon, S., Morales Maqueda, M. A., Legat, V., & Fichefet, T. (2009). An elastic-viscous-plastic sea ice model formulated on Arakawa B and C grids. *Ocean Modelling*, 27(3-4), 174–184. https://doi.org/10.1016/j.ocemod.2009.01.004
- Brown, K. A., Williams, W. J., Carmack, E. C., Fiske, G., François, R., McLennan, D., & Peucker-Ehrenbrink, B. (2020). Geochemistry of small Canadian Arctic Rivers with diverse geological and hydrological settings. *Journal of Geophysical Research: Biogeosciences*, 125(1), 1–21. https://doi.org/10.1029/2019JG005414
- Burgers, T. M., Azetsu-Scott, K., Punshon, S., Miller, L. A., Davelaar, M., Marriott, S., et al. (2024). Dissolved inorganic carbon (DIC), total alkalinity, water temperature, salinity and other hydrographic and chemical data collected from discrete samples and profile observations during the CCGS Amundsen AN1902, 2019 ArcticNet cruise Leg 2 (EXPOCODE 18DL20190530) in the Baffin Bay, Davis Strait, Northwestern Passages (eastern Canadian Arctic) from 2019-07-05 to 2019-08-15 (NCEI Accession 0290861). [Dataset]. NOAA National Centers for Environmental Information. https://doi.org/10.25921/1p3c-b750
- Burgers, T. M., Miller, L. A., Thomas, H., Else, B. G. T., Gosselin, M., & Papakyriakou, T. (2017). Surface water pCO₂ variations and sea-air CO₂ fluxes during summer in the eastern Canadian Arctic. *Journal of Geophysical Research: Oceans*, 122(12), 9663–9678. https://doi.org/10.1002/2017JC013250
- Burgers, T. M., Tremblay, J.-É., Else, B. G. T., & Papakyriakou, T. N. (2020). Estimates of net community production from multiple approaches surrounding the spring ice-edge bloom in Baffin Bay. *Elementa: Science of the Anthropocene*, 8(1), 013. https://doi.org/10.1525/elementa.013
 Carlson, D. F., Pasma, J., Jacobsen, M. E., Hansen, M. H., Thomsen, S., Lillethorup, J. P., et al. (2019). Retrieval of ice samples using the ice
- drone. Frontiers in Earth Science, 7(November), 1–14. https://doi.org/10.3389/feart.2019.00287
- Carmack, E. C., Yamamoto-Kawai, M., Haine, T. W. N., Bacon, S., Bluhm, B. A., Lique, C., et al. (2016). Freshwater and its role in the Arctic Marine System: Sources, disposition, storage, export, and physical and biogeochemical consequences in the Arctic and global oceans. *Journal of Geophysical Research: Biogeosciences*, 121(3), 675–717. https://doi.org/10.1002/2015JG003140
- Charette, M. A., Kipp, L. E., Jensen, L. T., Dabrowski, J. S., Whitmore, L. M., Fitzsimmons, J. N., et al. (2020). The transpolar drift as a source of riverine and shelf-derived trace elements to the central Arctic Ocean. *Journal of Geophysical Research: Oceans*, 125(5), e2019JC015920. https://doi.org/10.1029/2019JC015920
- Cooper, L. W., McClelland, J. W., Holmes, R. M., Raymond, P. A., Gibson, J. J., Guay, C. K., & Peterson, B. J. (2008). Flow-weighted values of runoff tracers (8¹⁸O, DOC, Ba, alkalinity) from the six largest Arctic rivers. *Geophysical Research Letters*, 35(18), L18606. https://doi.org/10.1029/2008GI.035007
- Cooper, L. W., Whitledge, T. E., Grebmeier, J. M., & Weingartner, T. (1997). The nutrient, salinity, and stable oxygen isotope composition of Bering and Chukchi Seas waters in and near the Bering Strait. *Journal of Geophysical Research*, 102(C6), 12563–12573. https://doi.org/10. 1029/97JC00015
- Courtois, P., Garcia-Quintana, Y., Hu, X., & Myers, P. G. (2020). Kinematic subduction rate of Labrador Sea water from an eddy-permitting numerical model. *Journal of Geophysical Research: Oceans*, 125(7), e2019JC015475. https://doi.org/10.1029/2019JC015475
- Curry, B., Lee, C. M., & Petrie, B. (2011). Volume, freshwater, and heat fluxes through Davis Strait, 2004 05. Journal of Physical Ocean-ography, 41(3), 429–436. https://doi.org/10.1175/2010JPO4536.1
- Curry, B., Lee, C. M., Petrie, B., Moritz, R. E., & Kwok, R. (2014). Multiyear volume, Liquid freshwater, and sea ice transports through Davis Strait, 2004–10. *Journal of Physical Oceanography*, 44(4), 1244–1266. https://doi.org/10.1175/JPO-D-13-0177.1

BURGERS ET AL. 19 of 21

- Dalton, A., Copland, L., Tivy, A., Van Wychen, W., & Cook, A. (2019). Iceberg production and characteristics around the prince of wales icefield, Ellesmere island, 1997-2015. Arctic Antarctic and Alpine Research, 51(1), 412–427. https://doi.org/10.1080/15230430.2019.1634442
- Dalton, A., Van Wychen, W., Copland, L., Gray, L., & Burgess, D. (2022). Seasonal and multiyear flow variability on the prince of wales icefield, Ellesmere island: 2009–2019. Journal of Geophysical Research: Earth Surface, 127(4), e2021JF006501. https://doi.org/10.1029/ 2021JF006501
- Dickson, A. G., Sabine, C. L., & Christian, J. R. (Eds.) (2007). In *Guide to best practices for ocean CO2 measurements. PICES Special Publication* (Vol. 3). North Pacific Marine Science Organization.
- Doney, S. C., Fabry, V. J., Feely, R. A., & Kleypas, J. A. (2009). Ocean acidification: The other CO₂ Problem. *Annual Review of Marine Science*, 1, 169–194. https://doi.org/10.1146/annurey.marine.010908.163834
- Escher, J. C. (1985). Geological map of Greenland, 1:500 000, Sheet 4, Upernavik Isfjord. https://doi.org/10.22008/FK2/YERETL
- Fairbanks, R. (1982). The origin of continental shelf and slope water in the New York Bight and Gulf of Maine: Evidence from H₂¹⁸O/H₂¹⁶O ratio measurements. *Journal of Geophysical Research*, 87(C8), 5796–5808. https://doi.org/10.1029/jc087ic08p05796
- Fichefet, T., & Morales Maqueda, M. A. (1997). Sensitivity of a global sea ice model to the treatment of ice thermodynamics and dynamics. Journal of Geophysical Research, 102(C6), 12609–12646. https://doi.org/10.1029/97jc00480
- Fransson, A., Chierici, M., Nomura, D., Granskog, M. A., Kristiansen, S., Martma, T., & Nehrke, G. (2015). Effect of glacial drainage water on the CO₂ system and ocean acidification state in an Arctic tidewater-glacier fjord during two contrasting years. *Journal of Geophysical Research: Oceans*, 120(4), 2413–2429. https://doi.org/10.1002/2014JC010320
- Friedlingstein, P., O'Sullivan, M., Jones, M. W., Andrew, R. M., Bakker, D. C. E., Hauck, J., et al. (2023). Global carbon budget 2023. Earth System Science Data. 15(12), 5301–5369. https://doi.org/10.5194/essd-15-5301-2023
- Garde, A. A., & Marker, M. K. (2010). Geological map of Greenland, 1:500 000, sheet 3, Kangerlussuaq/Søndre Strømfjord Nuussuaq (2nd ed.). https://doi.org/10.22008/FK2/X9U5BF
- Gattuso, J.-P., Epitalon, J.-M., Lavigne, H., & Orr, J. (2021). Seacarb: Seawater carbonate chemistry.
- Haine, T. W. N., Curry, B., Gerdes, R., Hansen, E., Karcher, M., Lee, C., et al. (2015). Arctic freshwater export: Status, mechanisms, and prospects. *Global and Planetary Change*, 125, 13–35. https://doi.org/10.1016/j.gloplacha.2014.11.013
- Henson, H. C., Holding, J. M., Meire, L., Rysgaard, S., Stedmon, C. A., Stuart-Lee, A., et al. (2023). Coastal freshening drives acidification state in Greenland fjords. Science of the Total Environment, 855(September 2022), 158962. https://doi.org/10.1016/j.scitotenv.2022.158962
- Holmes, R. M., Aminot, A., Kérouel, R., Hooker, B. A., & Peterson, B. J. (1999). A simple and precise method for measuring ammonium in marine and freshwater ecosystems. *Canadian Journal of Fisheries and Aquatic Sciences*, 56(10), 1801–1808. https://doi.org/10.1139/f99-128
- Hopwood, M. J., Carroll, D., Dunse, T., Hodson, A., Holding, J. M., Iriarte, J. L., et al. (2020). Review article: How does glacier discharge affect marine biogeochemistry and primary production in the Arctic? *The Cryosphere*, 14(4), 1347–1383. https://doi.org/10.5194/tc-14-1347-2020
- Hu, X., Myers, P. G., & Lu, Y. (2019). Pacific Water pathway in the Arctic Ocean and Beaufort Gyre in two simulations with different horizontal resolutions. *Journal of Geophysical Research: Oceans*, 124(8), 6414–6432. https://doi.org/10.1029/2019JC015111
- Hunke, E. C., & Dukowicz, J. K. (1997). An elastic-viscous-plastic model for sea ice dynamics. *Journal of Physical Oceanography*, 27(9), 1849–1867. https://doi.org/10.1175/1520-0485(1997)027<1849:aevpmf>2.0.co;2
- Jensen, H. M., Pedersen, L., Burmeister, A. D., & Hansen, B. W. (1999). Pelagic primary production during summer along 65 to 72°N off West Greenland. *Polar Biology*, 21(5), 269–278. https://doi.org/10.1007/s003000050362
- Johnson, K. M., Wills, K. D., Butler, D. B., Johnson, W. K., & Wong, C. S. (1993). Coulometric total carbon dioxide analysis for marine studies: Maximizing the performance of an automated gas extraction system and coulometric detector. *Marine Chemistry*, 44(1993), 167–187. https://doi.org/10.1016/0304-4203(93)90201-X
- Jones, E. P., Anderson, L. G., & Swift, J. H. (1998). Distribution of Atlantic and pacific waters in the upper Arctic Ocean: Implications for circulation. Geophysical Research Letters, 25(6), 765–768. https://doi.org/10.1029/98g100464
- Klein, B., LeBlanc, B., Mei, Z. P., Beret, R., Michaud, J., Mundy, C. J., et al. (2002). Phytoplankton biomass, production and potential export in the North Water. *Deep-Sea Research Part II Topical Studies in Oceanography*, 49(22–23), 4983–5002. https://doi.org/10.1016/S0967-0645 (02)00174-1
- Krawczyk, D. W., Kryk, A., Juggins, S., Burmeister, A., Pearce, C., Seidenkrantz, M. S., et al. (2021). Spatio-temporal changes in ocean conditions and primary production in Baffin Bay and the Labrador Sea. *Palaeogeography, Palaeoclimatology, Palaeoecology*, 563, 110175. https://doi.org/10.1016/j.palaeo.2020.110175
- Landy, J. C., Ehn, J. K., Babb, D. G., Thériault, N., & Barber, D. G. (2017). Sea ice thickness in the eastern Canadian Arctic: Hudson Bay complex and Baffin Bay. Remote Sensing of Environment, 200, 281–294. https://doi.org/10.1016/j.rse.2017.08.019
- Lauvset, S. K., Lange, N., Tanhua, T., Bittig, H. C., Olsen, A., Kozyr, A., et al. (2022). GLODAPv2.2022: The latest version of the global interior ocean biogeochemical data product [Dataset]. Earth System Science Data, 14(12), 5543–5572. https://doi.org/10.5194/essd-14-5543-2022
- Lehmann, N., Kienast, M., Granger, J., Bourbonnais, A., Altabet, M. A., & Tremblay, J.-É. (2019). Remote western Arctic nutrients fuel remineralization in deep Baffin Bay. Global Biogeochemical Cycles, 33(6), 649–667. https://doi.org/10.1029/2018GB006134
- Lin, P., Pickart, R. S., Torres, D. J., & Pacini, A. (2018). Evolution of the freshwater coastal current at the southern tip of Greenland. *Journal of Physical Oceanography*, 48(9), 2127–2140. https://doi.org/10.1175/JPO-D-18-0035.1
- Lueker, T. J., Dickson, A. G., & Keeling, C. D. (2000). Ocean pCO₂ calculated from dissolved inorganic carbon, alkalinity, and equations for K₁ and K₂: Validation based on laboratory measurements of CO₂ in gas and seawater at equilibrium. *Marine Chemistry*, 70(1–3), 105–119. https://doi.org/10.1016/s0304-4203(00)00022-0
- Madec, G. (2008). NEMO Ocean engine (No 27). France: Note du Pôle de Modélisation de l'Institut Pierre-Simon Laplace (IPSL).
- Meire, L., Søgaard, D. H., Mortensen, J., Meysman, F. J. R., Soetaert, K., Arendt, K. E., et al. (2015). Glacial meltwater and primary production are drivers of strong CO₂ uptake in fjord and coastal waters adjacent to the Greenland Ice Sheet. *Biogeosciences*, 12(8), 2347–2363. https://doi.org/10.5194/bg-12-2347-2015
- Melling, H., Agnew, T. A., Falkner, K. K., Greenberg, D. A., Lee, C. M., Münchow, A., et al. (2008). Fresh-water fluxes via pacific and arctic outflows across the Canadian polar shelf. In R. R. Dickson, J. Meincke, & P. Rhines (Eds.), Arctic-subarctic ocean fluxes: Defining the role of the northern seas in climate (pp. 193–247). Springer. https://doi.org/10.1007/978-1-4020-6774-7
- Mesinger, F., & Arakawa, A. (1976). Numerical methods used in Atmospheric models. GARP Publi.
- Miller, L. A., Papakyriakou, T. N., Collins, R. E., Deming, J. W., Ehn, J. K., MacDonald, R. W., et al. (2011). Carbon dynamics in sea ice: A winter flux time series. *Journal of Geophysical Research*, 116(C2), C02028. https://doi.org/10.1029/2009JC006058
- Mortensen, J., Rysgaard, S., Winding, M. H. S., Arendt, K. E., Lund, H., Stuart-Lee, A. E., & Meire, L. (2022). Multidecadal water mass dynamics on the West Greenland shelf. *Journal of Geophysical Research: Oceans*, 127(7), e2022JC018724. https://doi.org/10.1029/2022JC018724

BURGERS ET AL. 20 of 21



Journal of Geophysical Research: Oceans

- 10.1029/2024JC021122
- Mouginot, J., Rignot, E., Bjørk, A. A., van den Broeke, M., Millan, R., Morlighem, M., et al. (2019). Forty-six years of Greenland Ice Sheet mass balance from 1972 to 2018. *Proceedings of the National Academy of Sciences of the United States of America*, 116(19), 9239–9244. https://doi.org/10.1073/pnas.1904242116
- Mucci, A. (1983). The solubility of calcite and aragonite in seawater at various salinities, temperatures, and one atmosphere total pressure. American Journal of Science, 283(7), 780–799. https://doi.org/10.2475/ajs.283.7.780
- Myers, P. G. (2023). Pacific water circulation in Baffin bay from 1/12 degree NEMO model simulation. ERA (Education and Research Archive), University of Alberta. https://doi.org/10.7939/r3-rh6y-9q93
- Myers, P. G., Donnelly, C., & Ribergaard, M. H. (2009). Structure and variability of the West Greenland current in summer derived from 6 repeat standard sections. *Progress in Oceanography*, 80(1–2), 93–112. https://doi.org/10.1016/j.pocean.2008.12.003
- Myers, P. G., & Ribergaard, M. H. (2013). Warming of the polar water layer in Disko bay and potential impact on Jakobshavn Isbrae. *Journal of Physical Oceanography*, 43(12), 2629–2640. https://doi.org/10.1175/JPO-D-12-051.1
- Orr, J. C., Epitalon, J.-M., Dickson, A. G., & Gattuso, J.-P. (2018). Routine uncertainty propagation for the marine carbon dioxide system. *Marine Chemistry*, 207, 84–107. https://doi.org/10.1016/j.marchem.2018.10.006
- Papadimitriou, S., Thomas, D. N., Kennedy, H., Haas, C., Kuosa, H., Krell, A., & Dieckmann, G. S. (2007). Biogeochemical composition of natural sea ice brines from the Weddell Sea during early austral summer. *Limnology & Oceanography*, 52(5), 1809–1823. https://doi.org/10.4319/io.2007.52.5.1809
- Punshon, S., Azetsu-Scott, K., Sherwood, O., & Edinger, E. N. (2019). Bottom water methane sources along the high latitude eastern Canadian continental shelf and their effects on the marine carbonate system. *Marine Chemistry*, 212, 83–95. https://doi.org/10.1016/j.marchem.2019.
- Randelhoff, A., Oziel, L., Massicotte, P., Bécu, G., Galí, M., Lacour, L., et al. (2019). The evolution of light and vertical mixing across a phytoplankton ice-edge bloom. *Elementa: Science of the Anthropocene*, 7, 20. https://doi.org/10.1525/elementa.357
- Rantanen, M., Karpechko, A. Y., Lipponen, A., Nordling, K., Hyvärinen, O., Ruosteenoja, K., et al. (2022). The Arctic has warmed nearly four times faster than the globe since 1979. Communications Earth and Environment, 3(1), 168. https://doi.org/10.1038/s43247-022-00498-3
- Rysgaard, S., Boone, W., Carlson, D., Sejr, M. K., Bendtsen, J., Juul-Pedersen, T., et al. (2020). An updated view on water masses on the pan-West Greenland continental shelf and their link to proglacial fjords. *Journal of Geophysical Research: Oceans*, 125(2), e2019JC015564. https://doi.org/10.1029/2019jc015564
- Rysgaard, S., Glud, R. N., Sejr, M. K., Bendtsen, J., & Christensen, P. B. (2007). Inorganic carbon transport during sea ice growth and decay: A carbon pump in polar seas. *Journal of Geophysical Research*, 112(C3), C03016. https://doi.org/10.1029/2006JC003572
- Rysgaard, S., Mortensen, J., Juul-Pedersen, T., Sørensen, L. L., Lennert, K., Søgaard, D. H., et al. (2012). High air-sea CO₂ uptake rates in nearshore and shelf areas of Southern Greenland: Temporal and spatial variability. *Marine Chemistry*, 128–129, 26–33. https://doi.org/10.1016/j.marchem.2011.11.002
- Shadwick, E. H., Thomas, H., Gratton, Y., Leong, D., Moore, S. A., Papakyriakou, T., & Prowe, A. E. F. (2011). Export of pacific carbon through the Arctic Archipelago to the North Atlantic. *Continental Shelf Research*, 31(7–8), 806–816. https://doi.org/10.1016/j.csr.2011.01.014
- Smith, G. C., Roy, F., Mann, P., Dupont, F., Brasnett, B., Lemieux, J.-F., et al. (2004). A new atmospheric dataset for forcing ice-ocean models: Evaluation of reforecasts using the Canadian global deterministic prediction system. *Quarterly Journal of the Royal Meteorological Society*, 140(680), 881–894. https://doi.org/10.1002/qj.2194
- Sulpis, O., Lauvset, S. K., & Hagens, M. (2020). Current estimates of K₁* and K₂* appear inconsistent with measured CO₂ system parameters in cold oceanic regions. *Ocean Science*, 16(4), 847–862. https://doi.org/10.5194/os-16-847-2020
- Tang, C. C. L., Ross, C. K., Yao, T., Petrie, B., DeTracey, B. M., & Dunlap, E. (2004). The circulation, water masses and sea-ice of Baffin Bay. Progress in Oceanography, 63(4), 183–228. https://doi.org/10.1016/j.pocean.2004.09.005
- Wu, Y., Tang, C., & Hannah, C. (2012). The circulation of eastern Canadian seas. *Progress in Oceanography*, 106, 28–48. https://doi.org/10.1016/i.pocean.2012.06.005
- Yamamoto-Kawai, M., McLaughlin, F., & Carmack, E. (2013). Ocean acidification in the three oceans surrounding northern North America. Journal of Geophysical Research: Oceans, 118(11), 6274–6284. https://doi.org/10.1002/2013JC009157
- Yamamoto-Kawai, M., McLaughlin, F. A., Carmack, E. C., Nishino, S., & Shimada, K. (2008). Freshwater budget of the Canada basin, Arctic Ocean, from salinity, 8¹⁸O, and nutrients. *Journal of Geophysical Research*, 113(C1), C01007. https://doi.org/10.1029/2006JC003858
- Yamamoto-Kawai, M., McLaughlin, F. A., Carmack, E. C., Nishino, S., & Shimada, K. (2009). Aragonite undersaturation in the Arctic Ocean: Effects of ocean acidification and sea ice melt. *Science*, 326(5956), 1098–1100. https://doi.org/10.1126/science.1174190
- Yamamoto-Kawai, M., Tanaka, N., & Pivovarov, S. (2005). Freshwater and brine behaviors in the Arctic Ocean deduced from historical data of δ¹⁸O and alkalinity (1929-2002 A.D.). *Journal of Geophysical Research*, 110(C10), C10003. https://doi.org/10.1029/2004JC002793
- Zeidan, S., Walker, J., Else, B. G. T., Miller, L. A., Azetsu-Scott, K., & Walker, B. D. (2022). Using radiocarbon measurements of dissolved inorganic carbon to determine a revised residence time for deep Baffin bay. Frontiers in Marine Science, 9, 845536. https://doi.org/10.3389/fmars.2022.845536

References From the Supporting Information

Spreen, G., Kaleschke, L., & Heygster, G. (2008). Sea ice remote sensing using AMSR-E 89-GHz channels. *Journal of Geophysical Research*, 113(2), C02S03. https://doi.org/10.1029/2005JC003384

BURGERS ET AL. 21 of 21